NASA TECHNICAL NOTE

NASA TN D-6264

c. 1

NASA TN D-6264

ANALYTICAL STUDY OF THE EFFECTS OF GEOMETRIC CHANGES ON THE FLOW CHARACTERISTICS OF TANDEM-BLADED COMPRESSOR STATORS

by Nelson L. Sanger

Lewis Research Center
Cleveland, Ohio 44135

NATIONAL AERONAUTICS AND SPACE ADMINISTRATION • WASHINGTON, D. C. • MARCH 1971

1. Report No. NASA TN D-6264	2. Government Accession No.	3. Recipient's Catalog No.
4. Title and Subtitle ANALYTICAL STUDY OF THE EFFECTS OF GEOMETRIC CHANGES ON THE FLOW CHARACTERISTICS OF TANDEM-BLADED COMPRESSOR STATORS		5. Report Date March 1971 6. Performing Organization Code
7. Author(s) Nelson L. Sanger		8. Performing Organization Report No. E-5876
9. Performing Organization Name and Address Lewis Research Center National Aeronautics and Space Administration Cleveland, Ohio 44135		10. Work Unit No. 720-03 11. Contract or Grant No.
12. Sponsoring Agency Name and Address National Aeronautics and Space Administration Washington, D. C. 20546		13. Type of Report and Period Covered Technical Note 14. Sponsoring Agency Code

15. Supplementary Notes

16. Abstract

The effects of changes in geometry on the performance of 15 tandem-bladed stators is reported. Five geometrical parameters were evaluated for flow only in the two-dimensional plane. Using results from this study a tandem blade was designed for which the analytically calculated loss was relatively small. A parameter that approximated the incidence of the mean flow on the rear blade showed an ability to identify effective tandem blade configurations. Boundary-layer calculations indicated that the shorter chord length tandem blade segments could not sustain as high a suction surface diffusion as conventional solid blade sections.

17. Key Words (Suggested by Author(s)) Compressors; Turbomachinery; Turbomachine blades; Stator blades; Airfoil aerodynamics

18. Distribution Statement Unclassified - unlimited

19. Security Classif. (of this report)	20. Security Classif. (of this page)	21. No. of Pages	22. Price*
Unclassified	Unclassified	62	$3.00

*For sale by the National Technical Information Service, Springfield, Virginia 22151

CONTENTS

ANALYTICAL STUDY OF THE EFFECTS OF GEOMETRIC CHANGES ON THE FLOW CHARACTERISTICS OF TANDEM-BLADED COMPRESSOR STATORS

by Nelson L. Sanger

Lewis Research Center

SUMMARY

The effects of changes in geometry on the flow characteristics of 15 double circular arc tandem-bladed stators was investigated. All tandem blades studied possessed the same total camber, total chord, and inlet velocity triangles as a reference solid blade. The solid blade was designed for a moderately high blade loading (diffusion factor of 0.5). Only flow in the two-dimensional plane was considered.

Five geometrical parameters were evaluated: convergence of the channel between two tandem blade segments, the gap between segments, the overlap between segments, the ratio of rear blade segment camber to front blade segment camber, and the ratio of rear blade segment chord to front blade segment chord.

Most tandem configurations produced an analytical loss that was lower than the loss calculated for the reference solid blade. From the trends indicated by the analysis, it was possible to design a tandem blade having a relatively small loss and a surface velocity distribution free of rapid decelerations. The resulting configurations had front and rear blade chords of equal length and a ratio of rear to front blade camber of 2 to 1. The blades were separated by a relatively small gap, the overlap between the two blade segments was moderate, and the channel had a small convergence.

A parameter κ_{b-b} showed an ability to identify effective tandem blade section geometry. It provides an approximation of the incidence on the rear blade segment of the mean flow entering the channel region.

Variations in chord ratio indicated a direct relation between permissible blade surface velocity diffusion and chord length. The shorter chord length tandem blade segments could not sustain as high a diffusion as the longer chord solid blade section.

INTRODUCTION

Advanced air-breathing engines will require fans and compressors that are capable of handling more air and producing higher pressures than present technology offers. They will also have to be lighter and more compact.

Reducing the size and weight can be achieved by reducing the number of stages, the number of blades, or the diameter. Using any of these methods to reduce the size and weight, while increasing performance, results in more work per blade (increased loading). More work per blade is characterized by greater suction-surface velocity deceleration, which produces more rapid growth of the boundary layer. This results in larger losses and, in some cases, boundary-layer separation. Therefore, an important problem of advanced compressor design is the development of highly loaded blading combined with an effective means of boundary layer control.

One approach is to use a tandem blade in place of a single, solid blade. The overall loading is distributed over two or more separate blades and a new boundary layer is begun on each blade. The camber, chord, and orientation of the blades with respect to each other can be varied to produce combinations of loading (work split) and loss suitable to the application. Recent experimental evidence indicates that some tandem blade designs are capable of sustaining high loading while producing relatively small losses (refs. 1 to 4).

One of the practical difficulties involved in evaluating tandem blades is the very large number of geometric configurations that are possible. This creates the need for a systematic approach to evaluation. It is also preferable to make such a study by analytical means to avoid expensive and time-consuming experimental testing.

Analytical programs have been developed at the Lewis Research Center that permit a systematic evaluation of tandem blades. Both solid and tandem circular arc blade section coordinates are computed, and a computer plot of the blade is obtained (ref. 5). The computed coordinates are then used directly in a program to compute the velocities in the flow field and on the blade surfaces (refs. 6 and 7). Blade forces are computed using the surface velocity information (ref. 8). The boundary-layer growth on all blade surfaces is also computed using the surface velocity information (ref. 9). And the total pressure loss is calculated in a program using Stewart's method (ref. 10).

These programs were used to conduct an analytical study of the effects of geometry on a tandem blade stator performance. The results are reported herein. A reference solid blade section was designed using conventional methods (ref. 11) for a moderately high loading (diffusion factor, $D = 0.5$). Fifteen tandem blade configurations were designed. All had the same design inlet velocity triangle and overall camber as the reference solid blade section. The tandem configurations were systematically chosen to span a range of tandem blade geometrical parameters.

The effects of geometric changes were evaluated on the basis of such parameters as blade surface velocity diffusion, loss coefficient, and work split between blade segments, and also effects on the calculated flow field (streamlines). The study was limited to the two-dimensional flow plane and to double circular arc stator blade sections.

DESIGN

The stator blade section used in this study had a diffusion factor of $D = 0.5$, a fluid turning of 43.25°, and a solidity of 1.5. Double circular arc blade shapes were used throughout, and all blade sections lay on cylindrical surfaces. The inlet axial velocity was 250 feet per second (76.2 m/sec), and the entire flow field was subsonic. The axial velocity ratio through the blade row was 1.0.

For reference, a solid blade section was first designed using the design rules of reference 11. Tandem blade sections were then designed to have an identical inlet velocity triangle, solidity, overall camber, and total chord as the solid blade.

Blade geometry parameters used in the design of both the solid and tandem blades are defined in figure 1. Pertinent design parameters are summarized in table I and symbols are described in the appendix.

Solid Blade

The solid blade section was designed first. Using the value of $D = 0.5$ (ref. 12) and an exit flow angle of 0°, the diffusion factor equation was solved for the inlet flow angle. The design procedure of reference 11 was followed for double circular arc blades of maximum thickness to chord ratios of 0.08.

The blade coordinates on a cylindrical surface were obtained from a computer program described in reference 13. In the succeeding discussion the suction and pressure surfaces are referred to as surface S and surface P, respectively, for purposes of brevity.

Tandem Blades

The tandem blade sections are composed of two blade segments called the front segment and the rear segment. For purposes of brevity, the segment surfaces shall also be abbreviated: the suction and pressure surfaces of the front segment shall be referred to as surfaces SF and PF, respectively, and the suction and pressure surfaces of the rear segment shall be referred to as surfaces SR and PR, respectively (see fig. 1(b)).

In designing the tandem blades a double circular arc shape was also used for the tandem blade segments. Overall camber, solidity, total chord, and inlet velocity triangles were the same as the solid blade values. Values for maximum thickness, leading-edge radius, and trailing-edge radius expressed as percentages of local chord (i.e., of front or rear segment chords) were identical to analogous solid blade parameters expressed as percentages of total chord. Blade coordinates were obtained from the program of reference 5.

The tandem blade section designs permitted the effects of five tandem blade parameters to be studied (see fig. 2):

(1) Channel convergence, F - the ratio of inlet (capture area) to outlet area of the channel between the segments

(2) Overlap, L - the length of the channel from the leading-edge circle center of the rear segment to the trailing edge circle center of the front segment

(3) Gap, G - the width of the channel at its exit

(4) Camber ratio, ϕ_R/ϕ_F - the ratio of the camber angle of the rear segment to the camber angle of the front segment

(5) Chord ratio, C_R/C_F - the ratio of the rear segment chord to the front segment chord

Gap and overlap are referenced to the total chord to make all parameters dimensionless.

The range over which each parameter was varied is shown in table II. Obviously, a complete coverage of every combination of these parameters over the indicated ranges would require an extremely large number of configurations. And such an extensive study is beyond the scope of this investigation. Fifteen configurations were selected covering anticipated values of most interest. The procedure used was to set four of the parameters to reference values and vary the fifth parameter over the indicated range. The reference values used are $F = 1.4$, $L/C_T = 0.112$, $G/C_T = 0.056$, $\phi_R/\phi_F = 2.0$, and $C_R/C_F = 1.0$.

ANALYTICAL PROCEDURES

This section describes briefly the four analytical computer programs used in this study and the parameters used to evaluate the results. Inviscid velocity distributions (blade surface and midstream flow field) were obtained from an ideal flow program. The surface velocity distributions were used to compute boundary layer growth, from which, in turn, loss calculations were made.

In addition, pressure forces were calculated on all blade segments.

Ideal Flow Calculations

Two ideal flow programs were used: one for the solid blade (ref. 6), and the other for tandem blades (ref. 7). The programs solve the stream function equation by finite difference methods. The output includes surface velocities and blade-to-blade flow field velocities and fluid angles. The flow field is compressible, subsonic, two-dimensional, and nonviscous. A constant blade-to-blade stream channel height in the radial direction was used. A constant flow rate was chosen to provide an inlet axial velocity of 250 feet per second (76.2 m/sec). The inlet conditions were total pressure, 2078 pounds per square foot (9.94×10^4 N/m^2); total temperature, 520° R (289 K); and total density, 0.00233 slugs per cubic foot (1.203 kg/m^3).

The Kutta condition is not directly specified in these programs. Instead, the weight flow through the channel and the exit angle can be varied to change the position of the trailing-edge stagnation streamline. Plots of the trailing-edge stagnation streamlines show that, when the channel weight flow or exit angle is specified so that the velocity curves for the suction surface and pressure surface just meet at the trailing edge, the stagnation streamline is alined with the extension of the blade segment mean camber line.

Boundary-Layer Calculations

The surface velocities from the ideal flow programs are used to calculate boundary-layer growth (ref. 9). It was necessary to make some assumptions to insure uniform approach and comparable results.

One assumption was that the boundary layer was turbulent over the entire blade surface. In real compressors, high turbulence levels, surface roughness effects, and leading-edge effects act to force early transition or even separation and reattachment. Horlock reported that design of compressor blading for laminar flow does not appear to be possible (ref. 14). And in the same paper he cited the work of Gostelow (ref. 15) as showing that boundary layers in a compressor cascade (in which turbulence levels are lower than in actual compressors) could be calculated accurately by assuming them to be fully turbulent at all points.

A second assumption required is a value for initial thickness of a turbulent boundary layer. This is not easily determined. Accurate boundary-layer measurements on real blades (blade chords of 3 to 4 in. (7.64 to 10.2 cm)) are difficult, if not impossible, to obtain. For use in this investigation, measurements made by Becker (ref. 16) on a blade having a 5-foot (1.52-m) chord were scaled down. An initial displacement thickness of 0.0002 foot (0.00006 m) and momentum thickness of 0.000143 foot (0.000044 m) were used. These values were applied consistently to all blade configurations considered.

Although the absolute accuracy of the initial thicknesses cannot be guaranteed, the trends shown by the results should be reliable.

A final area in which an assumption was necessary is that of a separation criterion. In this study a critical value of the incompressible form factor, H_i of 2.4 was used as a measure of whether or where separation occurred. The value 2.4, chosen as a separation indicator, was not crucial. In most cases, whenever H_i exceeded 2.0, the slope of the H_i as a function of distance curve was sufficiently steep to insure rapid growth to 2.4 and beyond. The conclusions reached thus would not be substantially altered if the critical H_i were designated at some intermediate value between 2.0 and 2.4. Generally, $H_i = 2.4$ was exceeded only on the suction surface of the blade near the trailing edge. In such cases, the boundary-layer thickness required for the loss calculations was simply extrapolated to the trailing-edge station. For the short distances involved, there was probably little difference between the extrapolated thickness and the separated thickness.

Two other cases in which H_i exceeded 2.4 both involved pressure-surface boundary layers. When the rear blade segment encountered high negative incidence angles, they were accompanied by large pressure-surface decelerations in the leading-edge region. Separation of the turbulent boundary layer was indicated. It was assumed that because of the localized nature of the deceleration, the boundary layer would reattach. Following the region of steep deceleration, the boundary layer was reattached at an initial thickness of three times the value normally used.

The other case of pressure-surface boundary layer separation occurred in adverse gradients on surface PF of the high convergence configuration (F = 1.7 and 2.0). In this case the boundary-layer thickness was extrapolated until the region of favorable gradient was reached, and then it was reattached at the extrapolated thickness. Although there is no assurance that reattachment would actually occur, it was assumed to occur for analytical purposes so that a loss value could be computed.

Loss Calculations

Stewart's method (ref. 10) was used to calculate the total compressible flow loss due to blade friction, trailing-edge thickness, and downstream mixing. The total loss coefficient is defined as the total pressure loss across the blade row divided by the inlet dynamic head. Stewart expressed it in terms of boundary-layer thicknesses for a compressible fluid. Values of displacement and momentum thickness at the trailing-edge station on the pressure and suction surfaces of a blade were obtained from the boundary-layer program. The average exit velocity and average inlet and exit flow angles were obtained from the ideal flow program.

It was assumed that the wake of the front blade of a tandem blade would not impinge on either the boundary layer or the wake of the rear blade. Therefore, separate loss calculations, for the front and rear blades, were added to obtain the total loss of the tandem blade.

Force Calculations

The surface velocity distribution calculated in the ideal flow programs is used to compute the pressure forces on each blade segment (ref. 8). The surface velocities converted to pressure are integrated by the trapezoidal rule over each surface, and the resultant forces are resolved in the tangential and meridional directions. For tandem blades, ratios are calculated between forces on the rear and front blades.

Blade Evaluation Parameters

This section describes the methods and parameters used to evaluate flow conditions across the blade section. Most of the information, obtained from the velocity distributions along blade segment pressure and suction surfaces, was essential, not only for its own value, but also to compute the other blade evaluation parameters. The surface velocities show regions of acceleration and deceleration that aid in the interpretation of boundary-layer development and in the evaluation of the effect of channel geometry. In addition, the area enclosed by the surface velocity plots gives a qualitative measure of blade loading and the loading split between segments of a tandem blade. Regions of negative loading, usually located in the leading-edge region of a blade was due to negative incidence, are also apparent from the surface velocity plots.

A blade loading parameter can be computed from the surface velocity distributions. The maximum velocity on the suction surface of a blade divided by the trailing-edge velocity is defined as the diffusion velocity ratio, DVR = V_{max}/V_{out}. The DVR provides a relative measure of the degree of diffusion on a blade surface and, therefore, of the tendency of the boundary layer to separate. It is similar to the equivalent diffusion factor D_{eq} defined by Lieblein in reference 17. On conventional solid blades in cascade, Lieblein found a correlation between a sharp increase in losses at D_{eq} values 2.0 or greater.

Boundary-layer growth was calculated directly from blade segment surface velocity information. The parameters used to describe boundary-layer development have already been described. They are the displacement thickness δ^*, the momentum thickness θ, and the incompressible form factor H_i.

The total loss coefficient $\bar{\omega}_T$, was calculated from the trailing-edge values of the boundary-layer thicknesses on each blade segment surface. The sum of the front segment loss coefficient $\bar{\omega}_F$ and the rear segment loss coefficient $\bar{\omega}_R$ constitutes the total loss coefficient for the tandem blade $\bar{\omega}_T$.

Although the surface velocity distributions provide a qualitative measure of the loading split between tandem blade segments, a quantitative measure is given directly by the force calculations, namely, by the ratio between rear blade and front blade tangential forces, $(f_R/f_F)_\theta$. Since this parameter might become confused with previously noted loading parameters (e.g., DVR, D_{eq}, and D), it can be thought of as a work split (for rotating blade rows) or a circulation split (for stationary blade rows). For the sake of simplicity, it will be referred to herein as a work split, even though a stationary blade row is under consideration. Because the force calculations are based on ideal flow surface velocity and pressure distributions, the work split parameter $(f_R/f_F)_\theta$ does not take into account variations in pressure distribution caused by boundary-layer growth or separation.

The camber angles of the front and rear segments of a tandem blade are also useful for evaluation. They can be compared with the actual turning angles of each blade, $\Delta\beta_F$ and $\Delta\beta_R$, to determine effectiveness of the tandem combination (e.g., a blade having a camber of 60° and a calculated turning angle of 20° is obviously ineffective). The turning angles are determined from the blade-to-blade flow field calculations of the ideal flow programs.

And finally, an angle κ_{b-b} is used to approximate the incidence angle of the mean flow on the rear blade segment. The angle κ_{b-b} is defined as the difference between the direction of the meanline of the rear segment at the leading edge and the direction of the meanline of the front segment at the point of intersection with the line $F \times G$ (see fig. 2). The value of κ_{b-b} is an output of the blade coordinate program (ref. 5). Its significance will become apparent as the discussion proceeds.

RESULTS AND DISCUSSION

In this section the performance of the solid and tandem blade configurations is discussed. First, a brief evaluation of the solid blade and its performance is given. The performance of the 15 tandem configurations is then considered. The tandem configurations are grouped according to geometry, and each set of performance plots is preceded by a figure showing the blade forms. A tandem blade incorporating the best geometry observed was designed and evaluated. Its performance is considered. A transposed tandem blade, in which the channel is formed between the suction surface of the front segment and the pressure surface of the rear segment, is then evaluated. And finally, some general trends are discussed.

For each configuration studied a standard format of plots is presented. The types of plots included in this format are

(1) Velocity distributions on suction and pressure surfaces of front and rear blade segments

(2) Boundary-layer growth on the suction and pressure surfaces of front and rear blade segments, as measured by displacement thickness δ^* and incompressible form factor H_i

(3) Loss coefficient $\overline{\omega}$ on front and rear blade segments as computed from boundary-layer parameters and a total loss coefficient which is a summation of the individual blade segment losses

(4) The division of work input between front and rear blade segments (work split) as measured by the ratio of tangential forces $(f_R/f_F)_\theta$.

The plots are grouped according to the geometrical parameter varied. The data on the plots are generally self-explanatory, and each plot will not be discussed individually. Instead they will be used as necessary to illustrate certain general or specific trends. A summary of results for the ranges of variables considered is given in table III. This table concisely summarizes all the important results. The columns on the left side give the geometry variations, and the other columns summarize the aerodynamic performance parameters.

From the results certain trends will be indicated from which estimates of promising combinations of geometric parameters can be made. It should be recognized that the numerical value indicated as best for a particular parameter is best only at the reference values of the other parameters.

Solid Blade

The blade section geometry of two solid blades in cascade is shown in figure 3. For purposes of comparison the surface velocity distribution for the solid blade is presented in figure 4. The DVR on the suction surface was 1.58. Boundary-layer calculations indicated suction-surface boundary-layer separation ($H_i = 2.4$) at around 95 percent of chord (fig. 5). The theoretical calculated loss coefficient for the blade at design incidence was $\overline{\omega} = 0.0367$.

Tandem Blades

In theory, the tandem blade section offers the promise of flow loss reduction (as compared to solid blade flow loss) by (1) introducing a new boundary layer at some point along the overall blade row chord and (2) providing the opportunity to keep velocity diffusions

low on the surfaces of the individual blade segments, thereby inhibiting boundary-layer growth.

The results of this study show that these goals can be realized through proper orientation of the blade segments with respect to each other. When so oriented, the incidence angle on the rear blade segment is within certain limits so as to prevent large local accelerations and decelerations. The flow through the channel separating the two blade segments is smooth and constantly accelerating. And the velocity at the channel exit (front blade trailing edge) is high, which produces a low front blade suction-surface diffusion.

These factors can best be illustrated by examining the streamline diagrams for two flow configurations (fig. 6). The two configurations presented specifically show change in convergence but have significance of a general nature that will aid in interpreting other configurations.

In figure 6(a) the stagnation streamline, which divides the channel flow from the main flow, meets the rear blade on the suction surface (i.e., within the channel). This has two general effects.

First, it results in relatively large local accelerations and decelerations around the leading edge of the rear segment. Boundary-layer separation from the pressure surface with subsequent reattachment at a larger thickness is likely to occur. The accelerations and decelerations in the leading-edge region of the blade act to reduce the area under the surface velocity distribution (fig. 7(a)) and even result in a local region of "negative lift" This results in a shift of work or circulation, in this case, to the front blade.

The second effect is that the location of the stagnation streamline causes a distortion of the channel flow. Streamlines near the pressure surface of the front blade begin to diverge near the channel region causing large pressure-surface deceleration (fig. 7(a)). This can cause boundary-layer separation and blocking of the channel flow. Also, the location of the stagnation point on the rear blade suction surface results in low channel velocity throughout the channel including the front blade trailing-edge region. This causes high front blade suction-surface diffusions, increased boundary-layer growth, and correspondingly increased loss.

In figure 6(b) the stagnation streamline meets the rear blade on the leading-edge radius. This has two beneficial effects.

First, local acceleration and deceleration around the leading-edge region of the rear blade is minimized. Thus, local separation of the boundary layer is avoided, thereby permitting the orderly establishment and growth of the boundary layer on both blade surfaces. Also, the absence of regions of acceleration and deceleration on the rear blade results in a relatively large enclosed area under the surface velocity distribution (fig. 7(b)). This results in a shift of work (circulation) to the rear blade.

The second effect of the location of the stagnation point on the leading-edge radius is that flow accelerates smoothly through the channel. The streamlines in the channel region show little distortion, thereby minimizing any local deceleration on blade surfaces.

Furthermore, the velocity level is high throughout the channel length. This minimizes the front blade suction surface diffusion, boundary layer growth on both blade surfaces, and associated loss level. It is important to note the variations in the angle κ_{b-b}, which approximates the incidence angle of the mean flow on the rear blade segment. For figure 6(a) the high negative value of $\kappa_{b-b} = -23.5^{o}$ is in accordance with the high negative incidence indicated by the stagnation streamline of the rear blade. In figure 6(b) $\kappa_{b-b} = -5.5^{o}$ for which the slope of the stagnation streamline and surface velocity distribution appeared to be favorable. Therefore, in evaluating other configurations, the value of κ_{b-b} will give a relative indication of how the channel flow compares with conditions depicted in figures 6 and 7.

The next sections show how the various geometric parameters affect the desirable flow qualities discussed above.

Effect of Convergence

Convergence in channel flow path was varied from $F = 1.1$ to 2.0 (configurations 2 to 6 in table III). The variations in blade section geometry are shown in figure 8, and the effects on flow parameters are shown in figures 9 to 12.

For the reference values used, the results show that the configuration having the lowest convergence, $F = 1.1$, produced the best flow conditions. This configuration is the one used to illustrate desirable slot flow conditions in the previous section and shown in figure 6(b). The angle κ_{b-b} was -5.5^{o}, and the total loss coefficient $\bar{\omega}_T$ was a minimum for the range of convergence values considered.

As convergence increased, κ_{b-b} became progressively more negative, and flow conditions approached those described in the previous section (and fig. 6(a)) for the highly negative κ_{b-b}. The total loss coefficient $\bar{\omega}_T$ increased as F increased and was due primarily to an increase in front segment loss. The work-split parameter $(f_R/f_F)_\theta$ indicated that more work had to be done by the front segment as convergence increased. This was confirmed by an increase in suction surface diffusion on the front segment (DVR_F) as F increased.

Effect of Gap

The size of the channel exit gap was varied from $G/C_T = 0.027$ to 0.110 (configurations 7, 4, and 8 in table III). The variations in blade section geometry are shown in figure 13, and the effects on flow parameters are shown in figures 14 to 17.

For the reference values used, the results show that the configuration having the smallest gap, $G/C_T = 0.027$, produced the best flow conditions. The κ_{b-b} value for the

case was -9.8°, which resulted in a small degree of surface PR deceleration. The total loss coefficient $\bar{\omega}_T$ was the smallest loss recorded of the geometric configurations investigated.

Some reservations must be expressed about this configuration, despite its good indicated performance. First, a small region of local deceleration occurred on surface SR. It was not a serious disturbance since boundary-layer growth was not affected, but it does represent a potential problem area. If other geometric parameters were changed while the gap was kept small, the condition might become worse. Second, the diffusion on surface SR was severe enough to cause separation. And third, some deceleration was apparent on surface PR due to negative incidence on the rear blade.

As the gap was increased, the diffusion (DVR_F) on surface SF increased as did boundary-layer growth and front blade loss. Rear blade loss remained essentially constant. The value of κ_{b-b} grew sharply negative causing large velocity diffusion on surface PR.

The data indicate that the best flow conditions occur when the gap is small. And although the overall loss increased with gap size, it did not exceed the equivalent solid blade loss for any of the gap configurations.

In the preceding discussion it should be recognized that the gap values are the physical distances between blades and do not account for boundary-layer thickness. Nevertheless, since flow accelerates on both surfaces in the region of the channel, the boundary-layer thicknesses are relatively small, and would not significantly affect the values presented.

Effect of Overlap

Overlap of the blade segments was varied from $L/C_T = 0.053$ to 0.251 (configurations 9, 4, 10, and 11 in table III). The variations in blade section geometry are shown in figure 18, and the effects on flow parameters are shown in figures 19 to 22.

For the reference values used, the results show that the configuration having the largest overlap, $L/C_T = 0.251$, produced the best flow conditions. However, it should be noted that total loss levels and the value of κ_{b-b} remained essentially constant between overlap values of $L/C_T = 0.112$ and 0.251. The attractiveness of large overlap derives largely from the increase in front segment trailing-edge velocity with increase in overlap. This resulted in lower front segment suction-surface diffusions DVR_F and a decrease in boundary-layer growth and front segment loss. At the other extreme, small overlap not only was DVR_F large but the value of κ_{b-b} was highly negative (-24.4°) and caused a large deceleration on surface PR.

There are some reasons, however, why it appears desirable to qualify the above findings. At large overlaps ($L/C_T = 0.251$) the channel assumed a converging-diverging

cross section, thus producing a region of local deceleration on surface SR. More simple fabrication and assembly procedures are possible with smaller overlap. A final reason, not evident from data presented herein, is that small overlaps may show improved performance at smaller convergences than the reference value of 1.4. Preliminary indications from some unpublished data for $F = 1.1$ show that some acceptable surface velocity profiles can be expected at overlaps as low as $L/C_T = 0.053$ (which corresponded to a zero axial overlap). However, at small overlaps, the κ_{b-b} calculations are quite sensitive to small changes in other geometrical parameters. This complicates design and also means that special care must be taken in the fabrication and assembly to insure proper alinement of the blade segments.

Therefore, in summarizing the data on overlap it can be concluded that for the reference values used, overlaps in the range $L/C_T = 0.112$ to 0.251 are acceptable.

Effect of Camber Ratio

The ratio of rear blade segment to front blade segment camber was varied from $\phi_R/\phi_F = 1.0$ to 3.0 (configurations 12, 4, 13, and 14 in table III). The variations in blade section geometry are shown in figure 23, and the effects on flow parameters are shown in figures 24 to 27. Specifying camber ratio is a means of controlling the loading split or work split between the two segments of a tandem blade section. Changes in the work split as measured by the parameters $(f_R/f_F)_\theta$, DVR_R and DVR_R are obvious from table III. The configuration having $\phi_R/\phi_F = 1.0$ has the front segment more highly loaded than the rear, and, as ϕ_R/ϕ_F increases, the loading shifts from front to rear segment.

For the reference conditions used in this study, the camber ratio of 2.0 configuration probably is, overall, the most acceptable. First, the overall loss is the minimum for all camber ratio configurations. Second, the work split between blade segments is nearly evenly divided ($f_R/f_F = 0.8$). And finally, the suction surface diffusion DVR on the front blade segment is lower than that on the rear blade segment.

The $DVR_F < DVR_R$ condition is desirable from an operating range standpoint. As incidence changes, the DVR_F will no doubt change more rapidly than DVR_R. Therefore, if the DVR_F can be kept low, a larger stable operating range should be expected. Furthermore, from the boundary-layer plots it appears that $DVR = 1.32$ is the highest that the front segment can tolerate without some separation of the suction-surface boundary layer.

Although the data cited herein shows $\phi_R/\phi_F = 2.0$ to be an optimum value, it is recognized that a different set of reference conditions or some special application could alter the value somewhat.

Effect of Chord Ratio

The ratio of rear blade segment to front blade segment chord was varied from 1.0 to 3.0 (configurations 4, 15, and 16 in table III). The variations in blade section geometry are shown in figure 28, and the effects on flow parameters are shown in figures 29 to 32. The three cases were investigated to determine if variation in chord ratio would produce similar shifts in loading and loss as observed for variation in camber ratio. The chord ratio variation was carried out for a camber ratio of $\phi_R/\phi_F = 2.0$ and the other reference blade geometric values.

The configuration having a chord ratio of 1.0 produced the minimum total loss, although the $C_R/C_F = 2.0$ configuration showed only a slightly greater loss. Nevertheless, $C_R/C_F = 1.0$ appears more attractive because the DVR_F and boundary layer results show it to be the least likely to produce suction-surface separation from the front segment. This reduces the likelihood of a separated region from the front segment meeting and adversely affecting rear segment suction-surface boundary layer flow.

Change in chord ratio interjects an additional variable, chord length, into relationships between DVR, boundary layer and loss. Boundary-layer growth (and ultimately, loss) is dependent on both the diffusion and the distance over which it occurs. This is evident from boundary-layer and loss results shown in figures 31 and 32.

On the front blade a trade-off occurred. As chord ratio increased (C_F decreased) the suction-surface boundary layer showed an increasing tendency to separate. But the decreased chord length partially cancelled out this effect (less surface length for boundary layer to grow), and in addition, the pressure-surface boundary layer became thinner. The net effect was a relatively constant $\bar{\omega}_F$ with change in C_R/C_F.

On the rear blade the blade surface length increased, which allowed the boundary layer to grow to a greater thickness even though DVR decreased. Rear blade loss therefore increased, as did the total loss.

Selection of a chord ratio may depend on the specific application, whether, for example, range or low loss operation is desired. But, as in the case of camber ratio, it will be desirable to keep the loading on the front segment below a value that causes boundary-layer separation. This is particularly important if the separated region might impinge on the rear segment suction surface.

Application to Design

The foregoing results were used to design a tandem blade for low loss operation. A chord ratio of 1 and a camber ratio of 2 were selected. The gap was kept relatively small at $G/C_T = 0.04$, and a small convergence of 1.1 was chosen. (The resulting value of $\kappa_{b\text{-}b}$ was -4.6°.) Visual inspection of geometrical plots revealed that at the small

convergence, configurations having an overlap of L/C_T greater than 0.11 resulted in converging-diverging channel cross sections. Therefore, overlap was specified at $L/C_T = 0.11$.

A plot of the blade geometry is presented in figure 33, and the results of the flow analysis are shown in figures 34 and 35. The surface velocities show no rapid decelerations or local disturbances (fig. 34). The only potential problem area is the surface SR diffusion velocity ratio of 1.5. The boundary-layer curves indicate that separation does occur on surface SR, but very near the trailing edge (fig. 35). The calculated loss coefficient, $\bar{\omega}_T = 0.0268$, was nearly the lowest of all configurations investigated. The only one having a lower loss (configuration 7, $G/C_T = 0.027$) had boundary-layer separation and reattachment at the beginning of surface PR and a region of local deceleration on surface SR.

The prospects therefore appear good that low loss tandem blades can be designed using the guidelines established in this investigation.

Transposed Tandem

Several cases were investigated in which the blades were located so as to form a channel between the suction surface of the front segment and the pressure surface of the rear segment. These cases were referred to as transposed tandem blades, and one is shown in figure 36. It was thought that flow on the suction surface of the front segment would be accelerated near the trailing edge by the channel flow, thereby permitting higher front segment loading without risk of separation.

The surface velocity distribution (fig. 37) is fairly typical of the configurations investigated. The velocity diffusions over surfaces SR, PF, and SR are sufficiently high to insure rapid boundary-layer growth and probably separation, if not stall. This is particularly serious in the case of surface SF where separation would cause blockage of the channel and lead to sizeable flow disruption. Inclining the rear blade to produce convergence, and therefore flow acceleration in the channel so as to reduce surface SF diffusion, would place a high positive incidence on the rear blade. This would lead to even higher surface SR diffusions and most likely to stall of the rear blade. For these reasons, further investigation of the transposed tandem case did not appear profitable.

General Trends

In the preceding sections the effects of certain independent geometric variables on tandem blade flow characteristics were discussed. From these studies certain general observations relating to loss levels, the angle κ_{b-b}, and the diffusion velocity DVR can be made.

Loss levels. - It was previously mentioned that the absolute values of the losses calculated may differ from actual measured loss values because assumptions of boundary-layer thickness and behavior. But it should be valid to compare calculated loss values with each other, since the same assumptions and procedures were applied consistently to each configuration. It is noteworthy that loss values for most tandem blade configurations were lower than the loss level for the reference solid blade. Some were as much as 25 percent lower than the solid blade loss. Thus, on a two-dimensional plane, a moderately loaded tandem stator blade appears to be capable of turning fluid through an equal angle with lower loss than a solid blade.

The angle κ_{b-b}. - The angle designated by κ_{b-b} is an approximation of the incidence angle of the channel flow with respect to the rear blade. In the configuration evaluated in this study κ_{b-b} varied from -4.6° to -26.0°. The best configurations, as measured by the criteria of low loss and absence of large flow decelerations on front and rear blades, were those having κ_{b-b} values of -4.6° and -5.5°. As κ_{b-b} become more negative, particularly beyond -10°, the more critical flow conditions occurring on both front and rear blades generally resulted in poorer performance. Insofar as a recommended range of κ_{b-b} can be made, $\kappa_{b-b} = -4^{\circ}$ to -8° appears to be reasonable.

High negative κ_{b-b} values caused low velocities in the vicinity of the front blade trailing edge, thereby resulting in high surface SF diffusions and consequent boundary-layer separation. High negative κ_{b-b} values were associated with streamline distortion in the channel region, which caused deceleration on surface PF. (In some cases this produced separation in the channel itself.) Finally, high negative κ_{b-b} values caused poor rear blade leading-edge flows and resulted in boundary-layer separation on surface PR.

Ideal flow calculations made for some cases in which κ_{b-b} values fell in the range -4° to 0° (unpublished) showed local decelerations on surfaces within the channel. The quantitative effect on loss was not established since the cases were not carried through all programs. But the conditions might be expected to increase boundary-layer growth. It is one indication of some undesirable flow effects at κ_{b-b} values less negative than the -5° value suggested.

From this study, the angle κ_{b-b} has emerged as a parameter that can give some reasonable assurance of good channel flow. The κ_{b-b} value is an output of the blade coordinate program (ref. 5) that can accomodate a large number of configurations with a short running time and, thus, very economically. The angle κ_{b-b} therefore can be a

powerful tool for scanning large numbers of configurations encompassing a wide range of design variables. Only the most attractive configurations need then be selected for further study using the ideal flow, boundary layer, loss, and force programs. These programs require considerably more running time and expense.

It is recognized that κ_{b-b} has been applied to data of a limited range of variables. Additional studies covering other ranges of variables, for example, blade stagger overall blade camber, etc., are required to establish the general applicability of the parameter and critical values.

Diffusion velocity ratio, DVR. - The diffusion velocity ratio provides a measure of the degree of diffusion on a blade surface and, therefore, of the tendency of the boundary layer to separate. It is defined as the maximum velocity on the suction surface of a blade divided by the trailing-edge velocity. An examination of the DVR's on both solid and tandem blades allows a preliminary study of the relations of blade chord, DVR, and boundary-layer separation.

The solid blade suction surface had a DVR of 1.58, and boundary-layer separation occurred at about 95 percent of chord. It is assumed that reduction of DVR to about 1.55 would probably have avoided boundary-layer separation and reduced loss correspondingly.

For the majority of tandem blades (having $C_R/C_F = 1.0$) the chord lengths of the front and rear segments were about 50 to 60 percent of the length of the solid blade chord. An examination of the surface velocity distributions and boundary-layer plots for the tandem blade segments shows that suction-surface boundary-layer separation consistently occurs at lower values of DVR than for the solid blade. (The value of H_i used to determine separation was 2.4. But the conclusion to be reached is not dependent on choice of critical H_i.) Applying the same criterion of no separation to the individual tandem blade segments results in a comparable critical DVR of 1.35 for $C_R/C_F = 1.0$.

Some additional data are provided by the chord ratio study. For $C_R/C_F = 2$ and 3, the chord lengths of the rear blades are approximately 74 and 83 percent of the chord length of the solid blade. The boundary-layer data for surface SR indicate that postponing separation until the trailing edge would require DVR_R values just slightly higher than the values obtained in the $C_R/C_F = 1$ cases. Accordingly, the estimated critical DVR_R values are 1.41 and 1.45 for $C_R/C_F = 2$ and 3, respectively. The estimated critical values of DVR as a function of chord ratio are summarized in the following table:

Chord ratio, C_R/C_F	Local chord to solid blade chord ratio, C/C_{solid}, percent	Estimated critical diffusion ratio, DVR
1 (front and rear segments)	50 to 60	1.35
2 (rear segment)	74	1.41
3 (rear segment)	83	1.45
Solid	100	1.55

The conclusion to be drawn from this table is that the shorter tandem blade segments cannot be loaded to the same level as the longer solid blades. As might be expected, the diffusion and the length over which it occurs are related and together affect boundary-layer behavior. The critical DVR numbers of 1.55 to 1.35 are not suggested as some new numerical criteria. It is suggested only that loading limits established from data for solid blades having conventional chord lengths cannot be applied to the shorter tandem blade segment chords.

In addition, it should be noted that no comparison is intended to be made between the Lieblein D_{eq} value of 2.0 (ref. 17) and the DVR values represented in the preceding table. Lieblein considered the case of blades operating in the high loss regime near the stall limit where some blade separation is virtually assured. The requisite used in the present study, however, was that no separation occur on the blade surface.

CONCLUDING REMARKS

The effect on blade flow characteristics of five tandem blade geometrical parameters was analytically investigated. The five parameters, channel convergence, gap, overlap, rear-to-front segment camber ratio, and rear-to-front segment chord ratio, were varied systematically by means of 15 tandem blade configurations.

Each tandem stator blade was designed to have the same overall camber (58.8°), total chord length (0.333 ft; 0.102 m), solidity (1.5), and inlet velocity triangle as a reference solid stator blade. Design was accomplished using a computer program which generated tandem blade coordinates. Both solid and tandem blades were designed to turn the flow through an angle of 43.25°. This corresponded to a diffusion factor of $D = 0.5$ for the solid blade.

For each tandem blade configuration the following calculations were made:

1. Ideal flow calculations producing surface velocity distributions on both blade segments

2. Boundary-layer growth using velocity information from the ideal flow calculations
3. Blade segment loss coefficient based on boundary-layer thickness at blade segment trailing edge
4. Forces on each blade segment using velocity information from the ideal flow calculations.

Strictly speaking, the trends and recommended numerical values noted in this study apply only to the configuration evaluated. However, it is quite likely that the trends and values have general applicability. The degree of this applicability must be determined by further research.

The results of the study indicated that tandem blade sections had significantly lower loss coefficients than the solid blade when optimum combinations of geometry were used. Systematic variations of parameters indicated that best flow conditions occured when:

1. Convergence F was relatively small, $1.0 < F < 1.2$
2. Gap was relatively small, $0.027 < G/C_T < 0.056$
3. Overlap was relatively large, $0.112 < L/C_T < 0.251$.

Of these three parameters it appears most important to keep convergence small. There is some evidence that if $F < 1.2$ gap and overlap can be varied over a greater range with acceptable flow conditions.

For the flow conditions used in this study a camber ratio of 2.0 and a chord ratio of 1.0 provided the best relations of loss, work-distribution, and loading levels. With this combination total blade loss coefficient was relatively low, the tangential forces on front and rear segments were about equal, and loading level on the front segment suction surface was low enough so that no separation was indicated.

A parameter that gave a consistent indication of the effectiveness of various configurations was the angle $\kappa_{b\text{-}b}$. It provides an approximation of the incidence on the rear blade segment of the mean flow entering the channel region. Results indicated optimum flow conditions when $\kappa_{b\text{-}b}$ was approximately -5^{o}. At more negative values, particularly beyond -10^{o}, flow conditions deteriorated sharply. There was also some evidence that when $\kappa_{b\text{-}b}$ was more positive than -5^{o}, some undesirable local decelerations of flow occurred. Further study is needed to establish the general applicability of the parameter itself and of the value -5^{o}. The parameter is of special interest because it can be obtained directly from the blade coordinate program, a program having short running time and therefore low expense.

As a result of variation in chord ratio, a direct relation between permissible blade surface velocity diffusion and chord length was observed. The shorter chord length of

the tandem blade segments could not sustain as high a diffusion as the longer chord solid blade section before separation of the blade surface boundary layer occurred.

Lewis Research Center,
National Aeronautics and Space Administration,
Cleveland, Ohio, December 3, 1970,
720-03.

APPENDIX - SYMBOLS

C	blade chord length, ft; m
D	diffusion factor (ref. 12)
D_{eq}	equivalent diffusion factor (ref. 17)
DVR	diffusion velocity ratio, V_{max}/V_{out}
F	channel convergence, ratio of gap at inlet to gap at outlet of channel (fig. 2)
f	force on blade surface, lb; N
G	gap between blade segments (fig. 2), ft; m
H_i	incompressible form factor (ref. 9)
i	incidence angle, i.e., angle between entrance flow direction and line tangent to blade section (segment) meanline at leading edge, deg
L	overlap between blade segments (fig. 2), ft; m
l.e.	leading edge
PF	pressure surface, front blade segment
PR	pressure surface, rear blade segment
RI	leading edge radius of blade segment, ft (m)
RO	trailing edge radius of blade segment, ft (m)
SF	suction surface, front blade segment
SR	suction surface, rear blade segment
t	thickness of blade, ft; m
te	trailing edge
V	velocity, ft/sec; m/sec
z	axial coordinate, ft (m)
β	fluid angle with respect to axial direction, deg
$\Delta\beta$	fluid turning angle, deg
δ^*	displacement thickness of boundary layer, ft; m
θ	momentum thickness of boundary layer, ft; m
κ	blade angle with respect to axial direction, deg
$\kappa_{b\text{-}b}$	angle between tangents to mean camber lines of rear blade segment and front blade segment at the points of intersection with the line containing F × G (fig. 2), deg
σ	blade solidity, i.e., chord to spacing ratio
ϕ	blade camber, deg
$\bar{\omega}$	blade loss coefficient, i.e., total pressure loss to inlet dynamic pressure

Subscripts:

F	front blade segment
in	blade inlet condition

max	maximum
out	conditions at blade trailing edge
R	rear blade segment
T	total or overall conditions
θ	tangential direction

REFERENCES

1. Bettner, James L.; and Nosek, Stanley M.: Summary of Tests on Two Highly Loaded Turbine Blade Concepts in Three-Dimensional Cascade Sector. Paper 69-WA/GT-5, ASME, Nov. 1969.

2. Linnemann, H.: Tandem Grid in a Single Stage Blower. Rep. RSIC-276, Redstone Sci. Information Center, Army Missile Command, Sept. 1964. (Available from DDC as AD-606782.)

3. Railly, J. W.; and El-Sarha, M. E.: An Investigation of the Flow Through Tandem Cascades. Proc. Inst. Mech. Eng., vol. 180, pt. 3J, 1965-1966, pp. 66-73.

4. Lueders, H. G.; and Roelke, R. J.: Some Experimental Results of Two Concepts Designed to Increase Turbine Blade Loading. Paper 69-WA/GT-1, ASME, Nov. 1969.

5. McNally, William D.; and Crouse, James E.: Fortran Program for Computing Coordinates of Circular Arc Single and Tandem Turbomachinery Blade Sections on a Plane. NASA TN D-6020, 1970.

6. Katsanis, Theodore; and McNally, William D.: Revised FORTRAN Program for Calculating Velocities and Streamlines on a Blade-to-Blade Stream Surface of a Turbomachine. NASA TM X-1764, 1969.

7. Katsanis, Theodore; and McNally, William D.: FORTRAN Program for Calculating Velocities on a Blade-to-Blade Stream Surface of a Tandem Blade Turbomachine. NASA TN D-5044, 1969.

8. McNally, William D.: FORTRAN Program for Calculating Aerodynamic Forces from Pressure or Velocity Distributions on Blade Sections. NASA TM X-2123, 1970.

9. McNally, William D.: FORTRAN Program for Calculating Compressible Laminar and Turbulent Boundary Layers in Arbitrary Pressure Gradients. NASA TN D-5681, 1970.

10. Stewart, Warner L.: Analysis of Two-Dimensional Compressible-Flow Loss Characteristics Downstream of Turbomachine Blade Rows in Terms of Basic Boundary-Layer Characteristics. NACA TN 3515, 1955.

11. Johnsen, Irving A.; and Bullock, Robert O., eds.: Aerodynamic Design of Axial-Flow Compressors. NASA SP-36, 1965.

12. Lieblein, Seymour; Schwenk, Francis C.; and Broderick, Robert L.: Diffusion Factor for Estimating Losses and Limiting Blade Loadings in Axial-Flow-Compressor Blade Elements. NACA RM E53D01, 1953.

13. Crouse, James E.; Janetzke, David C.; and Schwirian, Richard E.: A Computer Program for Composing Compressor Blading from Simulated Circular-Arc Elements on Conical Surfaces. NASA TN D-5437, 1969.

14. Horlock, J. H.: Some Recent Research in Turbo-Machinery. Proc. Inst. Mech. Eng., vol. 182, p. 1, no. 26, 1967-1968, pp. 571-594.

15. Gostelow, J. P.: The Accurate Prediction of Cascade Performance. Ph. D. thesis, Univ. Liverpool.

16. Becker, John V.: Boundary-Layer Transition on the N.A.C.A. 0012 and 23012 Airfoils in the 8- Foot High-Speed Wind Tunnel. NACA WR-L-682, 1940.

17. Lieblein, Seymour: Loss and Stall Analysis of Compressor Cascades. J. Basic Eng., vol. 81, no. 3, Sept. 1959, pp. 387-400.

TABLE I. - SUMMARY OF DESIGN PARAMETERS

(a) Solid blade

Total camber, ϕ_T, deg	58.8
Total chord, C_T, ft; m	0.333; 0.102
Maximum thickness to chord ratio, T_{max}/C_T	0.08
Leading-edge radius to chord ratio, RI/C_T	0.01
Trailing-edge radius to chord ratio, RO/C_T	0.0075
Inlet fluid angle, β_{in}, deg	43.25
Incidence angle, i, deg	-3.0
Solidity, σ	1.5
Diffusion factor, D	0.5

(b) Tandem blades

Total camber, ϕ_T, deg	58.8
Total chord, C_T, ft; m	0.333; 0.102
Maximum thickness to chord ratio	
Front blade, $T_{max,F}/C_F$	0.08
Rear blade, $T_{max,R}/C_R$	0.01
Leading-edge radius to chord ratio	
Front blade, RI_F/C_F	0.01
Rear blade, RI_R/C_R	0.01
Trailing-edge radius to chord ratio	
Front blade, RO_F/C_F	0.0075
Rear blade, RO_R/C_R	0.0075
Inlet fluid angle, β_{in}, deg	43.25
Incidence angle, i, deg	-3.0
Overall solidity, σ	1.5

TABLE II. - RANGE OF VARIATION OF TANDEM BLADE GEOMETRICAL PARAMETERS

Geometrical parameter	Range of parameter
Channel convergence, F	1.1, 1.2, [a]1.4, 1.7, 2.0
Overlap to chord ratio, G/C_T	0.053, [a]0.112, 0.178, 0.251
Gap to chord ratio, L/C_T	0.027, [a]0.056, 0.110
Camber ratio, ϕ_R/ϕ_F	1.0, 1.5, [a]2.0, 3.0
Chord ratio, C_R/C_F	[a]1.0, 2.0, 3.0

[a]Values correspond to reference tandem blade.

TABLF III. - SUMMARY OF RESULTS

Parameter varied	Configuration	Chord ratio, $C_R\ C_F$	Camber ratio, ϕ_R/ϕ_F	Gap to chord (total) ratio, G/C_T	Gap to chord (local) ratio, $G\ C_F$	Overlap to chord (total) ratio, $L\ C_T$	Overlap to chord (local) ratio, $L\ C_F$	Channel convergence, F	κ_{b-b}, deg	Front blade camber, θ_F, deg	Rear blade camber, θ_R, deg	Front blade fluid turning, $\Delta\beta_F$, deg	Rear blade fluid turning $\Delta_i\beta_R$, deg	Front blade loss coefficient, $\bar{\omega}_F$	Rear blade loss coefficient, $\bar{\omega}_R$	Total loss coefficient, $\bar{\omega}_T$	Diffusion velocity ratio		Ratio of tangential forces, $f_R/f_{F\ \theta}$
																	Front blade, DVR_F	Rear blade, DVR_R	
Solid blade	1	---	---	-----	----	-----	---	---	-----	58.8	----	----	----	----	------	------	0.0367	1.58	----	----
Channel convergence	2	1.0	2.0	0.056	0.1	0.113	0.2	1.1	-5.5	23.0	46.0	21.3	31.3	0.0093	0.0183	0.0276	1.19	1.50	1.30
	3	↓	↓	↓	↓	.111	↓	1.2	-7.5	24.0	48.1	21.8	29.0	.0114	.0184	.0298	1.24	1.48	1.13
	4					.111		1.4	-11.5	26.2	52.4	21.3	24.5	.0142	.0165	.0307	1.32	1.51	.80
	5					.111		1.7	-17.5	29.3	58.6	21.5	20.0	.0210	.0162	.0372	1.41	1.51	.60
	6					.111		2.0	-23.5	32.3	64.7	19.8	17.5	.0321	.0126	.0447	1.68	1.38	.52
Gap	7	1.0	2.0	0.027	0.05	0.114	0.2	1.4	-9.8	24.0	48.1	22.5	27.0	0.0105	0.0160	0.0265	1.20	1.45	0.96
	4	1.0	2.0	.056	.10	.112	.2	↓	-11.5	26.2	52.4	21.3	24.5	.0142	.0165	.0307	1.32	1.51	.80
	8	1.0	2.0	.110	.20	.110	.2		-26.0	30.3	60.7	19.3	21.8	.0203	.0159	.0362	1.52	1.44	.73
Overlap	9	1.0	2.0	0.053	0.1	0.053	0.1	1.4	-24.4	28.7	57.4	21.8	24.4	0.0216	0.0173	0.0389	1.70	1.50	0.77
	4	↓	↓	.056	↓	.112	.2	↓	-11.5	26.2	52.4	21.3	24.5	.0142	.0165	.0307	1.32	1.51	.80
	10			.059		.178	.3		-11.7	26.2	52.3	23.8	26.8	.0119	.0170	.0289	1.21	1.41	.87
	11			.063		.251	.4		-11.9	26.9	53.9	24.8	30.5	.0114	.0164	.0278	1.18	1.31	1.0
Camber	12	1.0	1.0	0.056	0.1	0.112	0.2	1.4	-7.6	39.2	39.2	30.8	20.0	0.0184	0.0152	0.0336	1.50	1.35	.40
	4	↓	1.5	↓	↓	↓	↓	↓	-9.9	31.4	47.1	24.5	23.5	.0173	.0166	.0339	1.42	1.43	.60
	13		2.0						-11.5	26.2	52.4	21.3	24.5	.0142	.0165	.0307	1.32	1.51	.80
	14		3.0						-13.3	19.6	58.9	16.3	29.0	.0122	.0234	.0356	1.21	1.52	1.30
Chord	4	1.0	2.0	0.056	0.10	0.112	0.2	1.4	-11.5	26.2	52.4	21.3	24.5	0.0142	0.0165	0.0307	1.32	1.51	.80
	15	2.0	2.0	.056	.15	.112	.3	1.4	-10.8	25.8	51.7	18.0	32.8	.0117	.0199	.0316	1.42	1.39	1.26
	16	3.0	2.0	0.056	.20	.112	.4	1.4	-8.2	25.9	51.7	16.3	35.7	.0125	.0236	.0361	1.48	1.42	1.47
Low loss tandem design	17	1.0	2.0	0.04	0.07	0.11	0.20	1.1	-4.6	22.6	45.3	----	----	0.0105	0.0163	0.0268	1.17	1.50	----

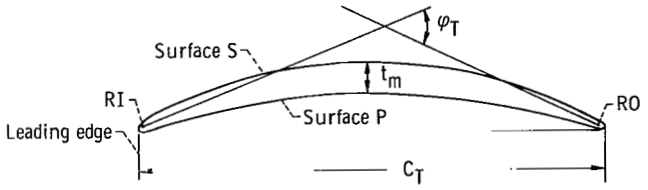

(a) Solid blade.

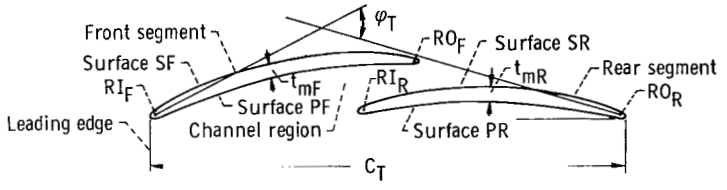

(b) Tandem blade.

Figure 1. - Nomenclature for solid and tandem blades.

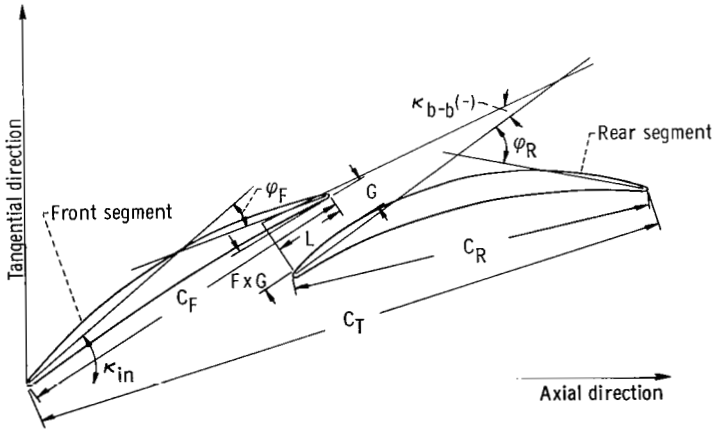

Figure 2. - Tandem blade geometric variables.

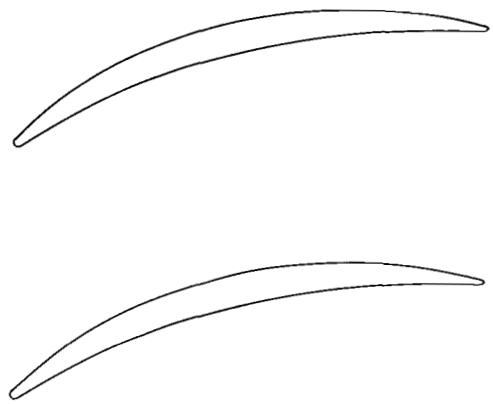

Figure 3. - Solid blade section geometry.

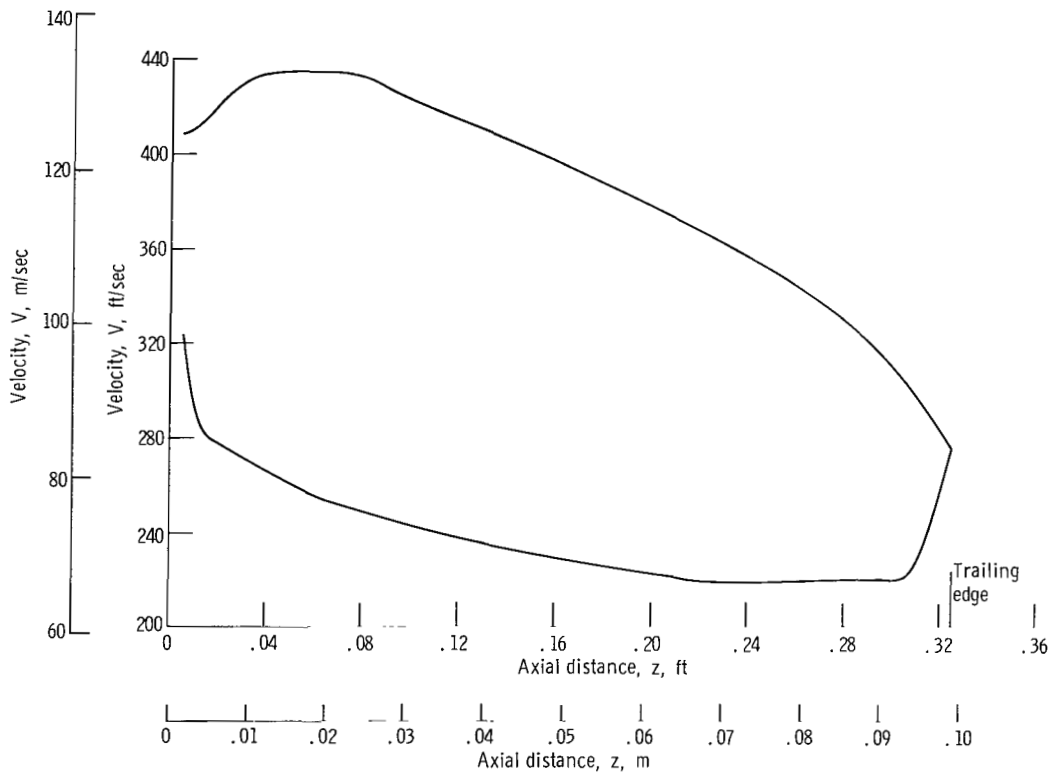

Figure 4. - Surface velocity profile on solid blade. Diffusion velocity ratio, 1.58.

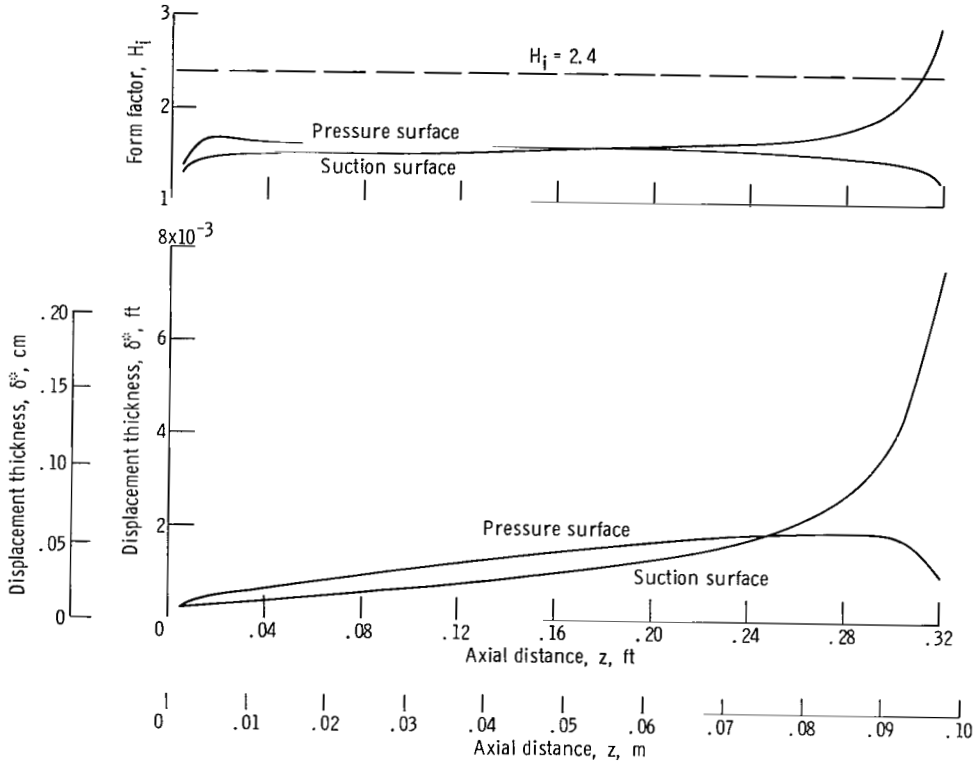

Figure 5. - Boundary-layer development on solid blade.

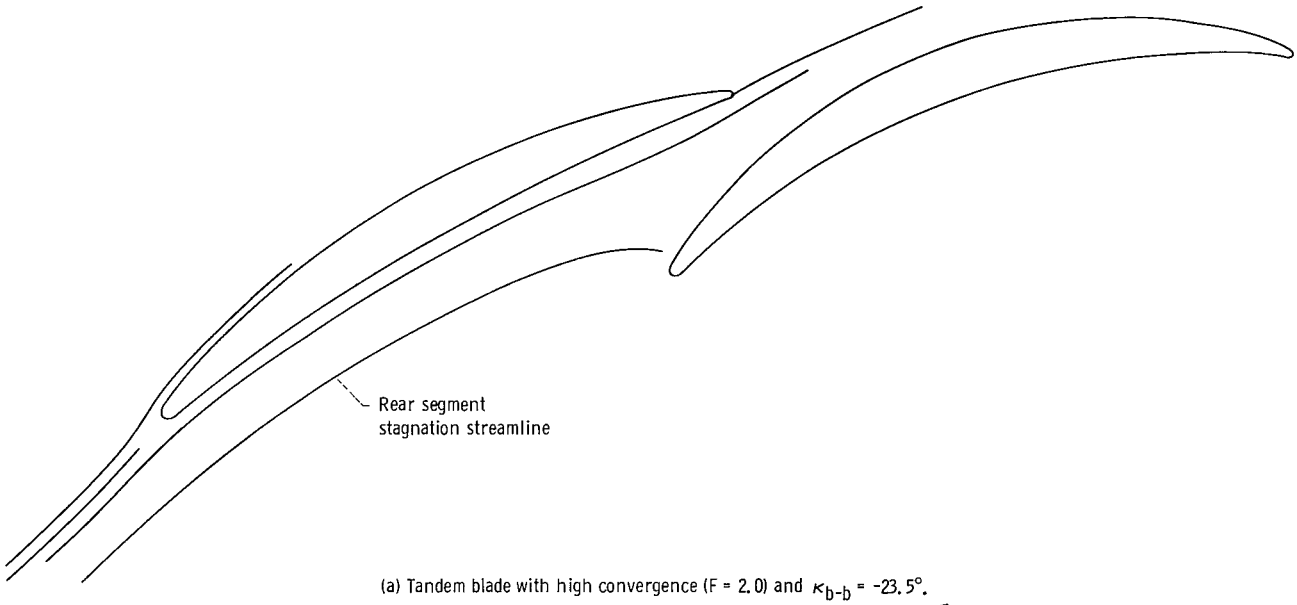

(a) Tandem blade with high convergence (F = 2.0) and $\kappa_{b-b} = -23.5°$.

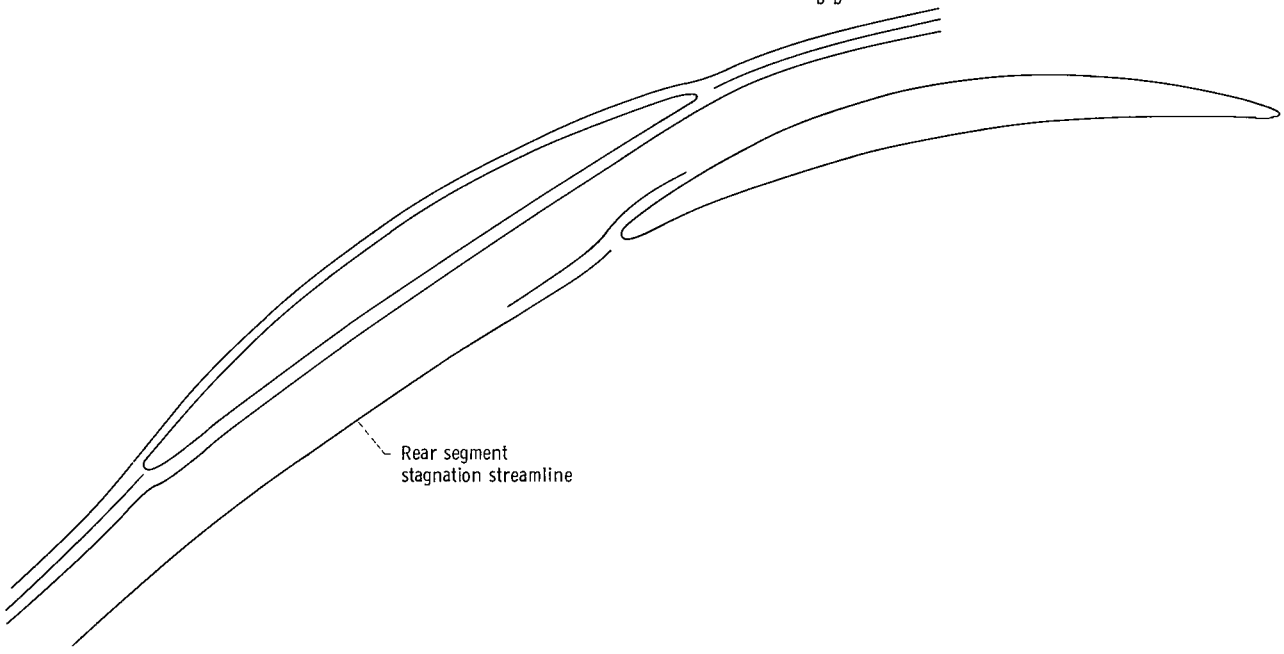

(b) Tandem blade with low convergence (F = 1.1) and $\kappa_{b-b} = -5.5°$.

Figure 6. - Streamline diagrams.

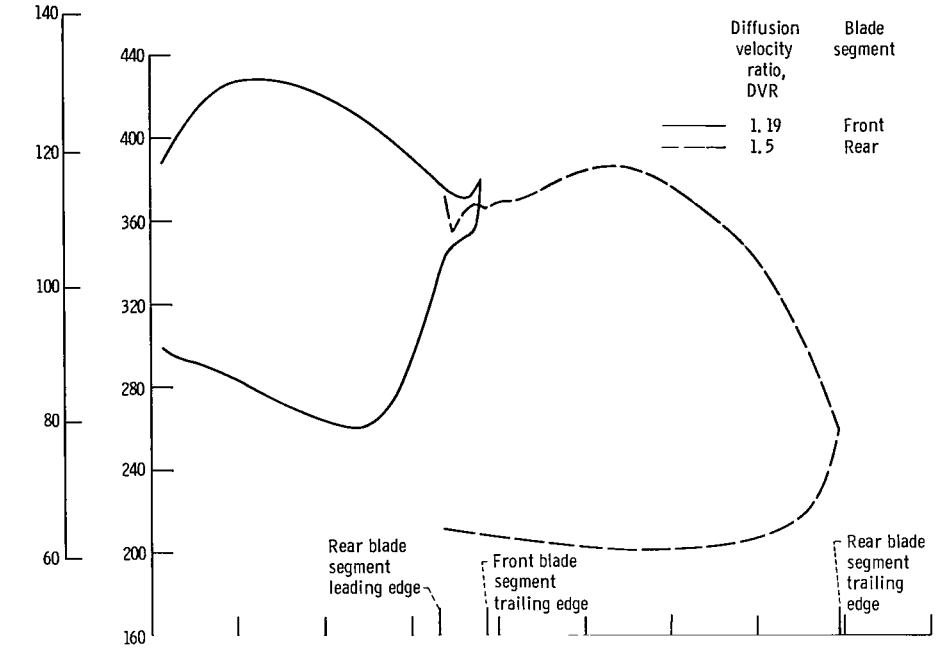

(a) Low convergence (F = 1.1); $\kappa_{b-b} = -5.5°$.

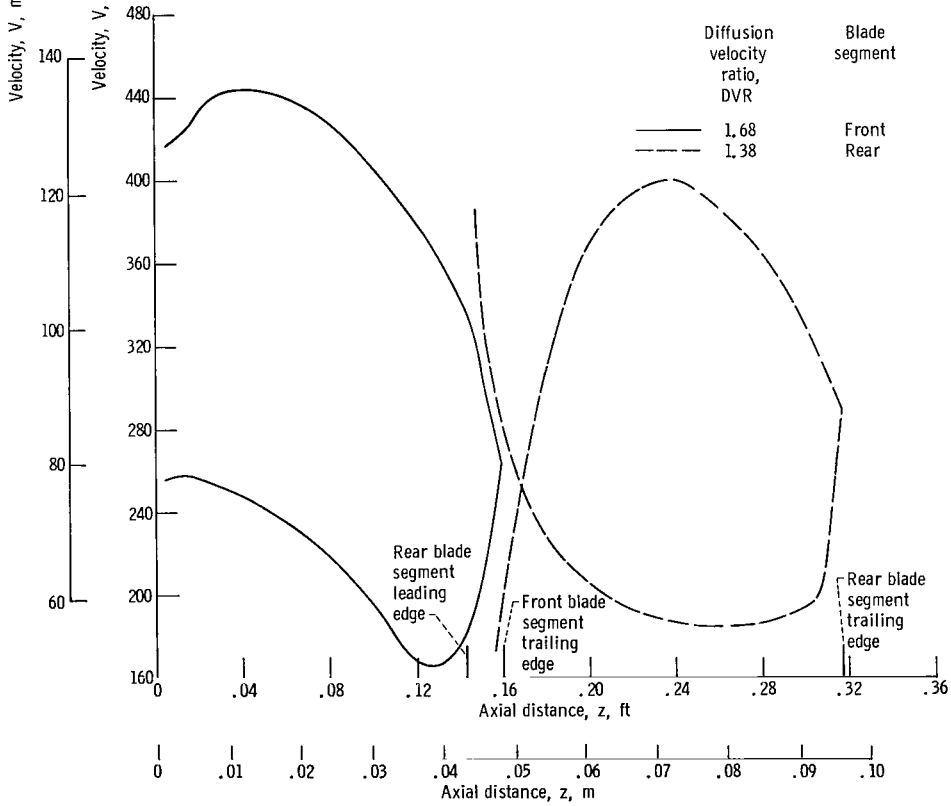

(b) High convergence (F = 2.0); $\kappa_{b-b} = -23.5°$.

Figure 7. - Surface velocity profile for tandem blade.

(a) Convergence, 1.1.

(b) Convergence, 1.2.

(c) Convergence, 1.4.

(d) Convergence, 1.7.

(e) Convergence, 2.0.

Figure 8. - Tandem blade section geometry: effect of channel convergence. Chord ratio, 1.0; camber ratio, 2.0; gap to chord ratio, 0.056; overlap to chord ratio, 0.112.

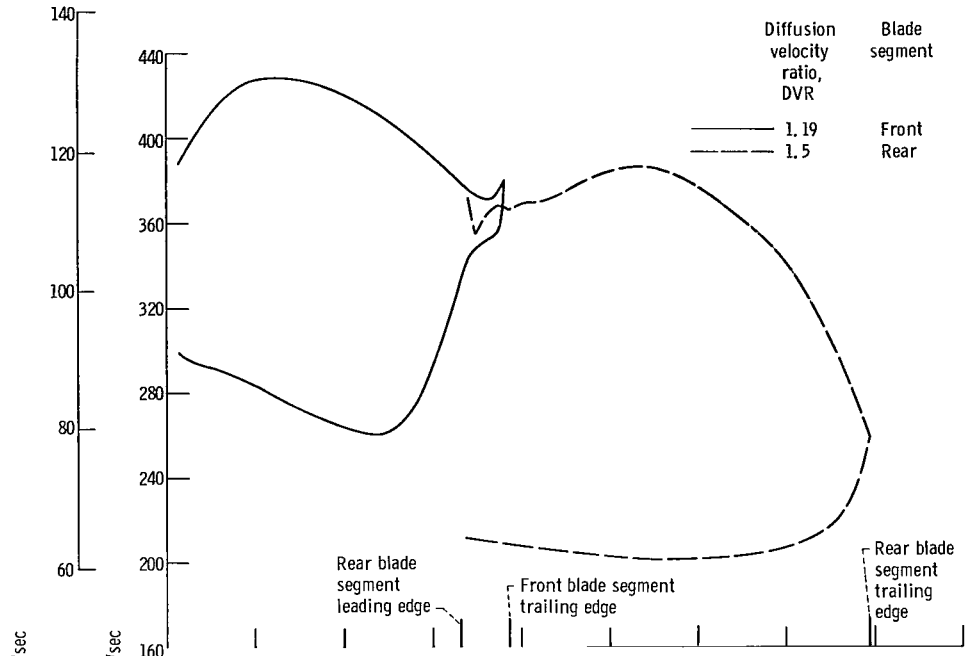

(a) Convergence, 1.1; $\kappa_{b\text{-}b} = -5.5°$.

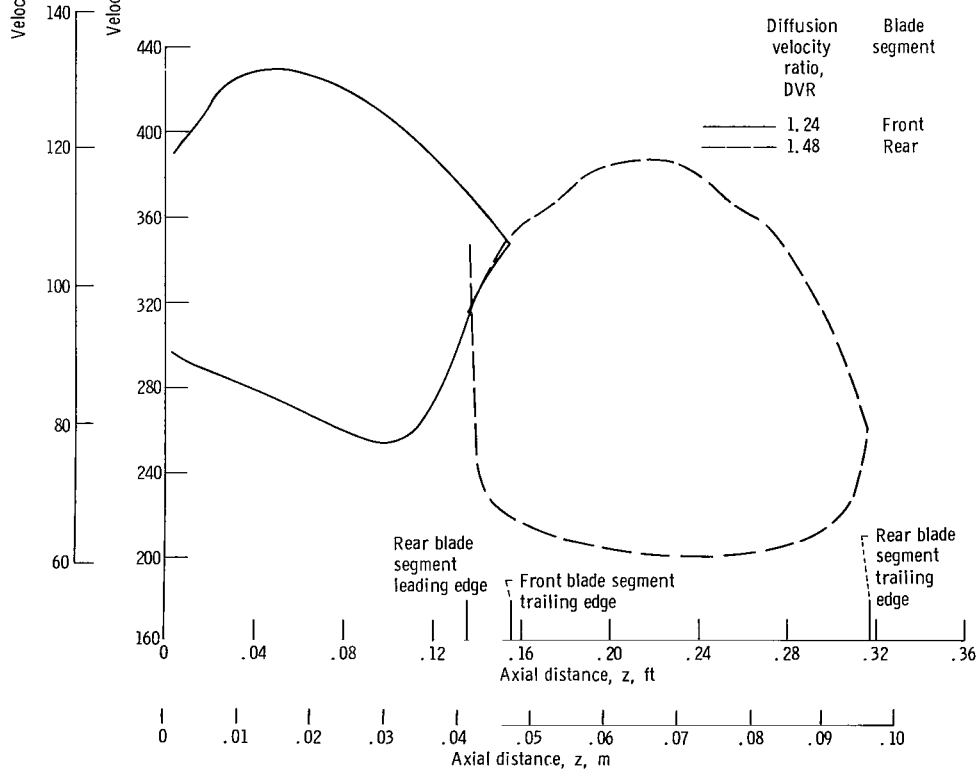

(b) Convergence, 1.2; $\kappa_{b\text{-}b} = -7.5°$.

Figure 9. - Effect of convergence on surface velocity profiles. Chord ratio, 1.0; camber ratio, 2.0; gap to chord ratio, 0.056; overlap to chord ratio, 0.112.

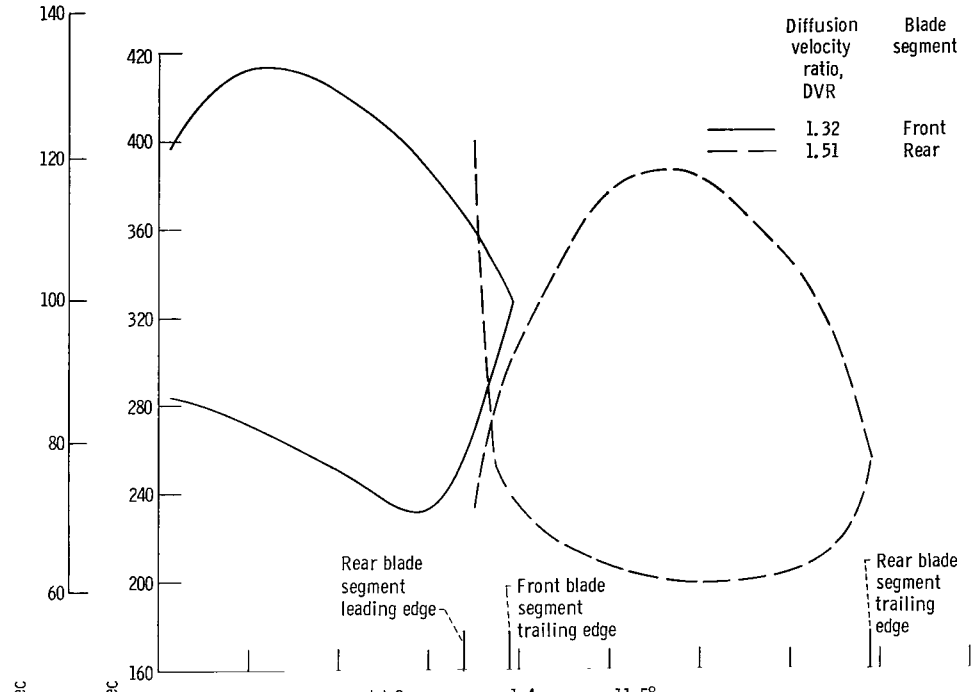

(c) Convergence, 1.4; $\kappa_{b-b} = -11.5°$.

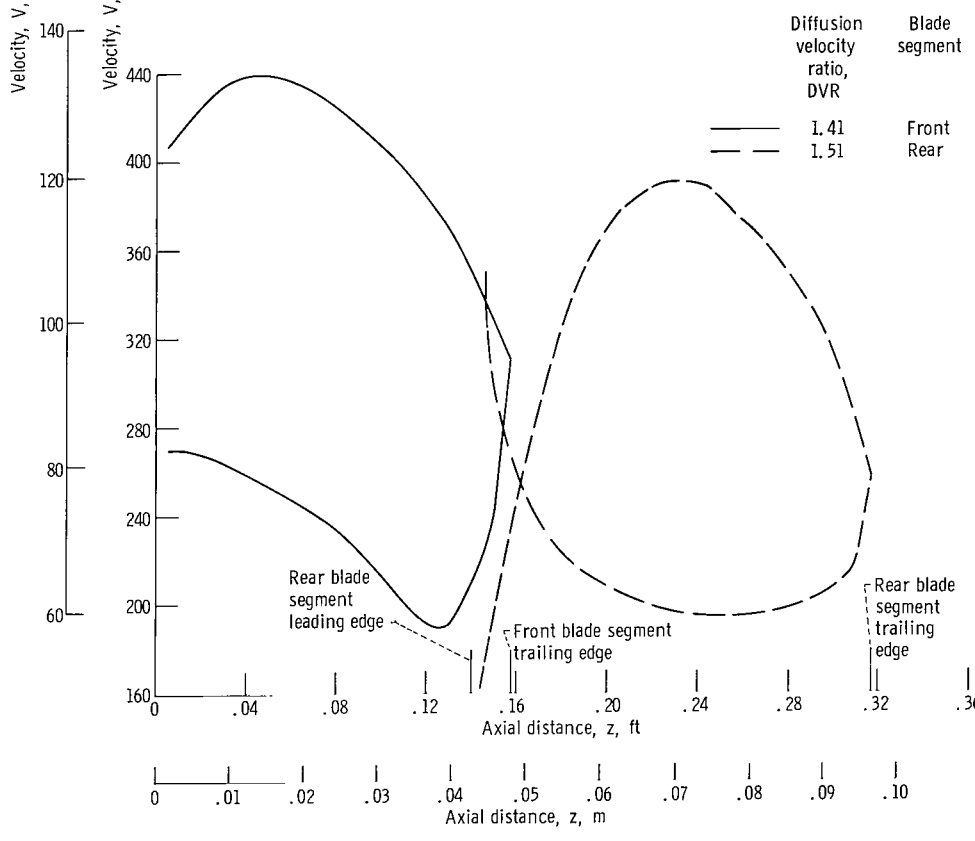

(d) Convergence, 1.7; $\kappa_{b-b} = -17.5°$.

Figure 9. - Continued.

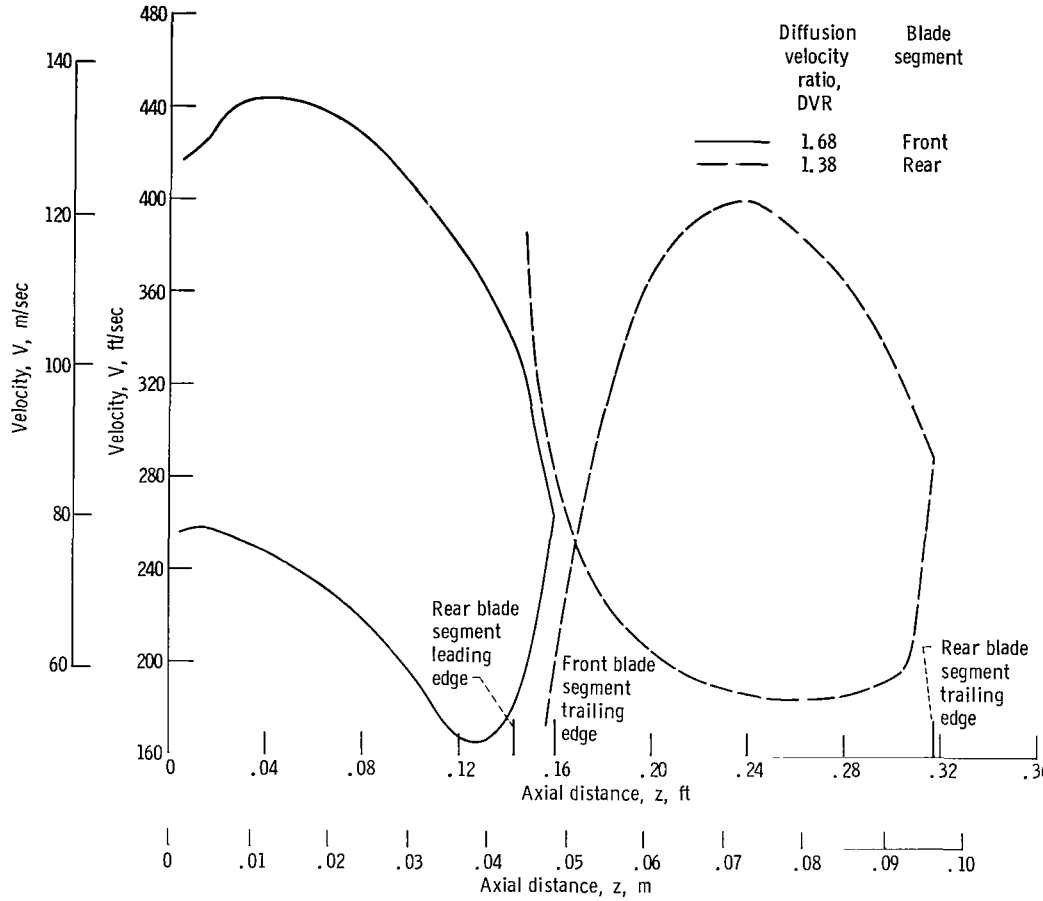

(e) Convergence, 2.0; $\kappa_{b-b} = 23.5°$.

Figure 9. - Concluded.

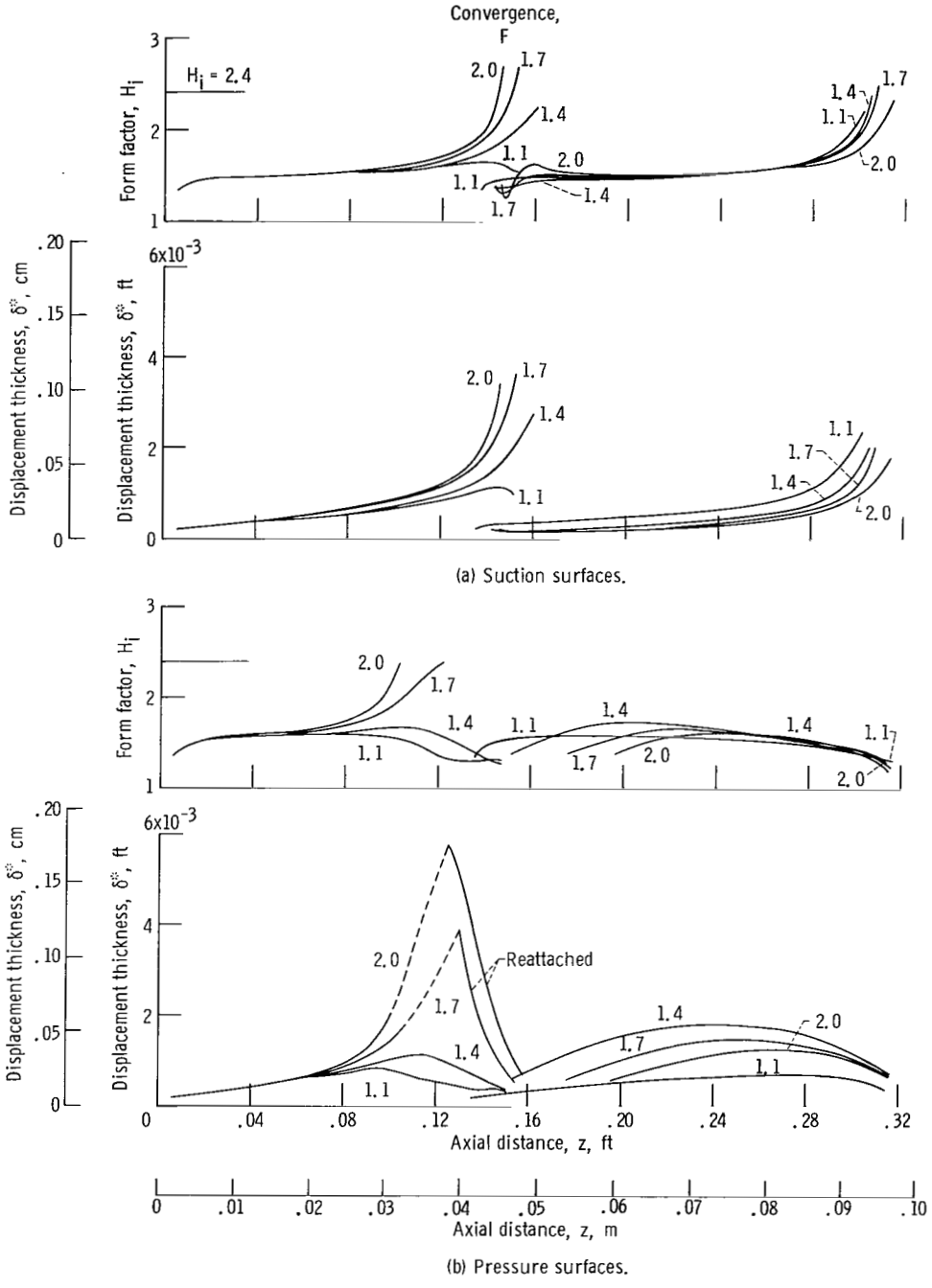

Figure 10. - Effect of channel convergence on boundary-layer development. Chord ratio, 1.0; camber ratio, 2.0; gap to chord ratio, 0.056; overlap to chord ratio, 0.112.

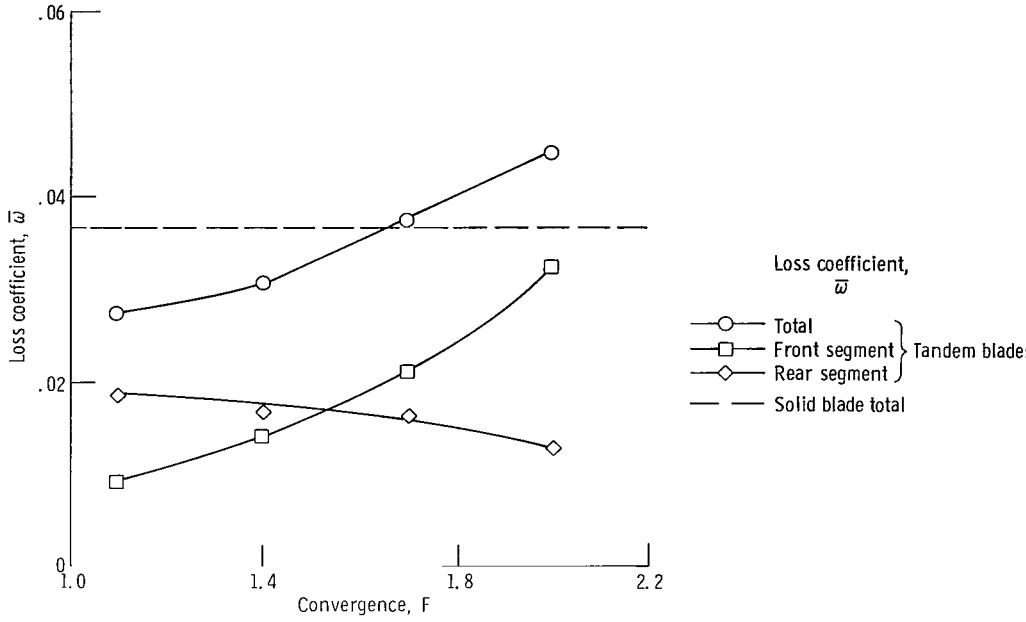

Figure 11. - Effect of convergence on loss. Chord ratio, 1.0; camber ratio, 2.0; gap to chord ratio, 0.056; overlap to chord ratio, 0.112.

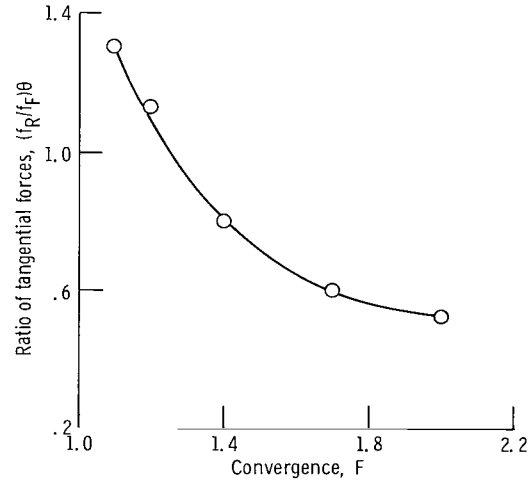

Figure 12. - Effect of convergence on work split. Chord ratio, 1.0; camber ratio, 2.0; gap to chord ratio, 0.056; overlap to chord ratio, 0.112.

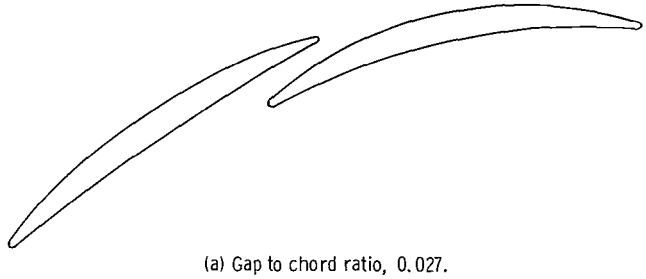

(a) Gap to chord ratio, 0.027.

(b) Gap to chord ratio, 0.056.

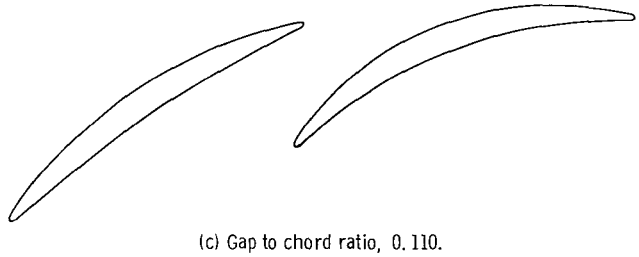

(c) Gap to chord ratio, 0.110.

Figure 13. - Tandem blade section geometry: effect of gap. Chord ratio, 1.0; camber ratio, 2.0; channel convergence, 1.4; overlap to chord ratio, 0.112.

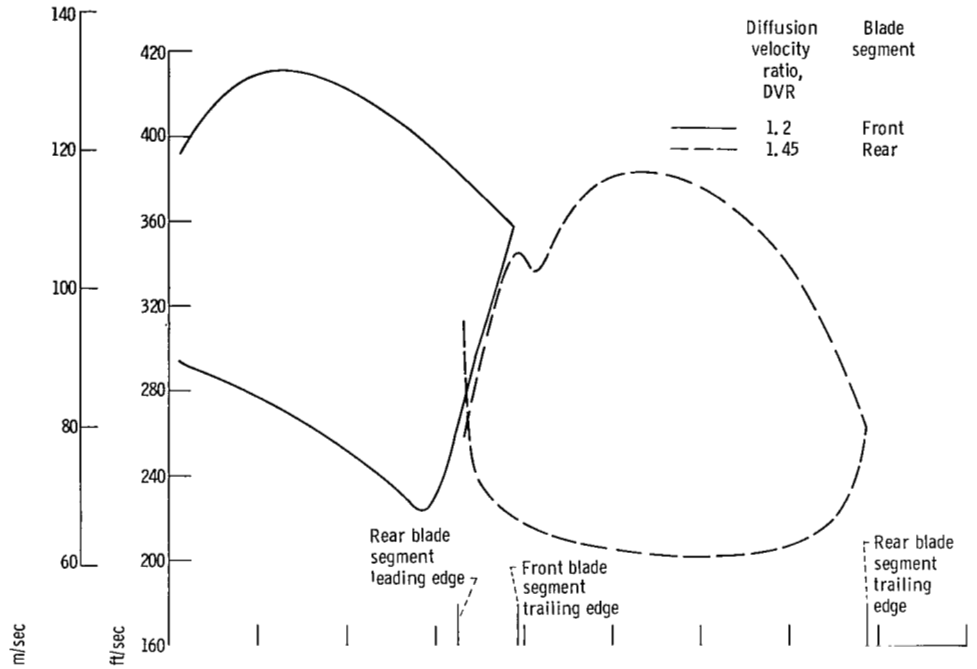

(a) Gap to chord ratio, 0.027; $\kappa_{b-b} = -9.8°$.

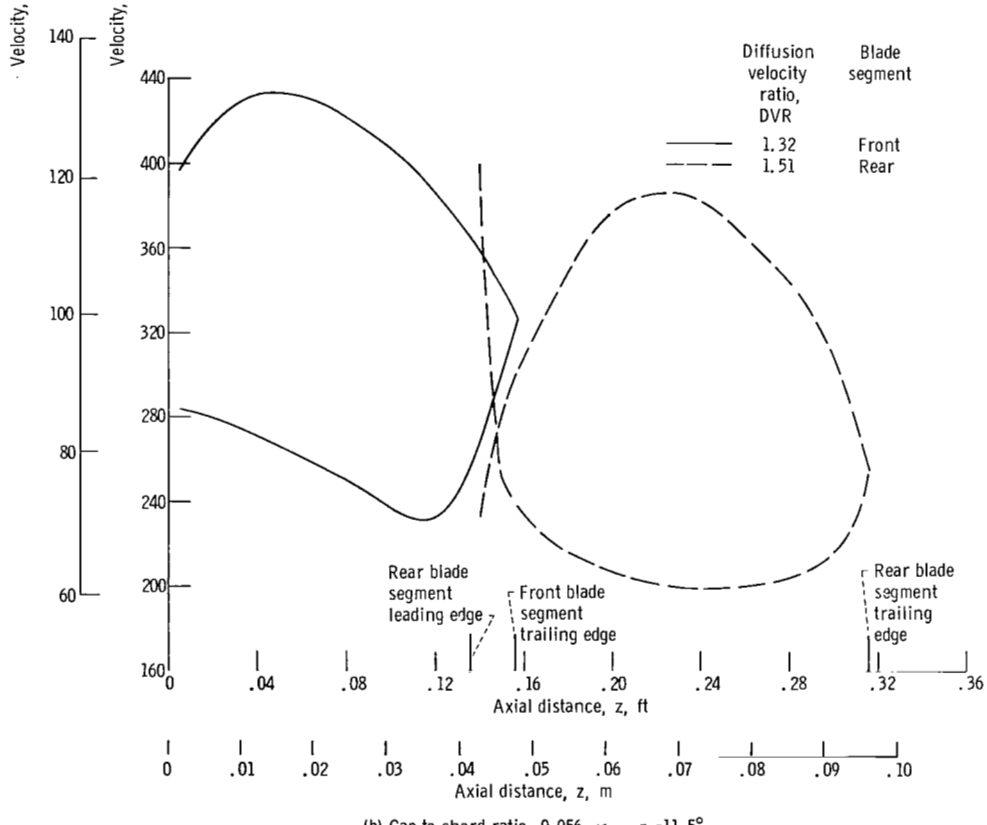

(b) Gap to chord ratio, 0.056; $\kappa_{b-b} = -11.5°$.

Figure 14. - Effect of gap on surface velocity profiles. Chord ratio, 1.0; camber ratio, 2.0; convergence, 1.4; overlap to chord ratio, 0.112.

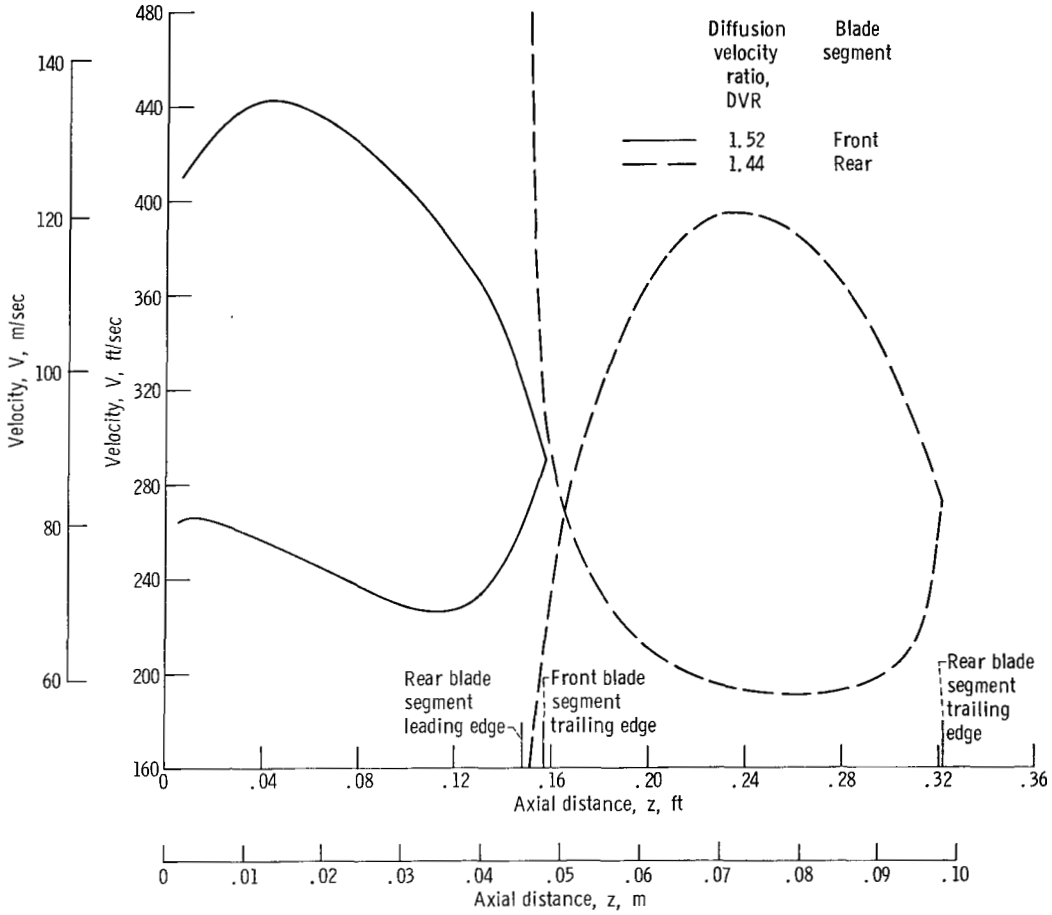

(c) Gap to chord ratio, 0.110; $\kappa_{b\text{-}b} = -26.0°$.

Figure 14. - Concluded.

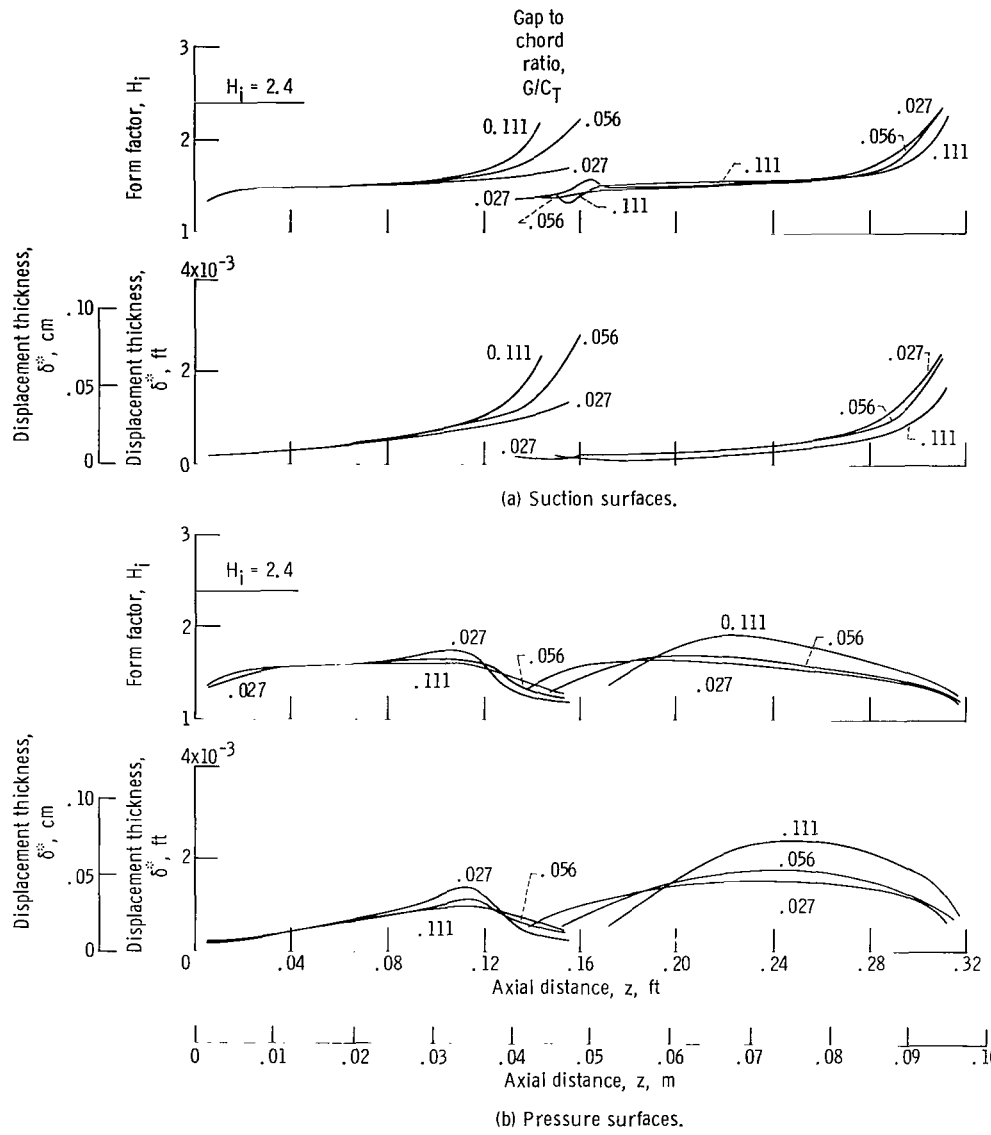

Figure 15. - Effect of gap on boundary-layer development configurations 4, 7, and 8. Chord radio, 1.0; camber ratio, 2.0; convergence, 1.4; overlap to chord ratio, 0.112.

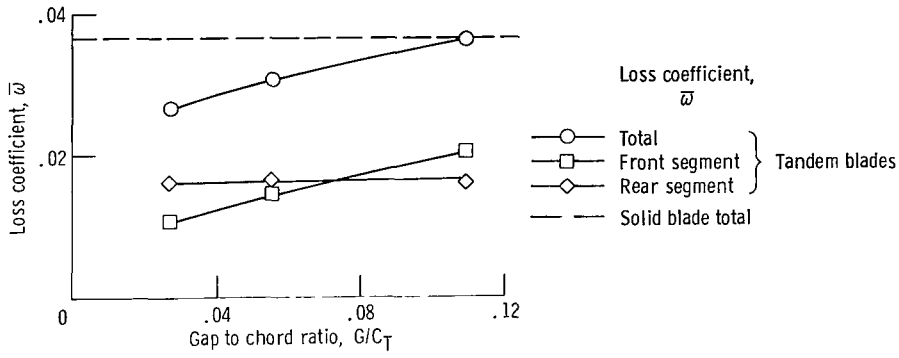

Figure 16. - Effect of gap on loss. Chord ratio, 1.0; camber ratio, 2.0; convergence, 1.4; overlap to chord ratio, 0.112.

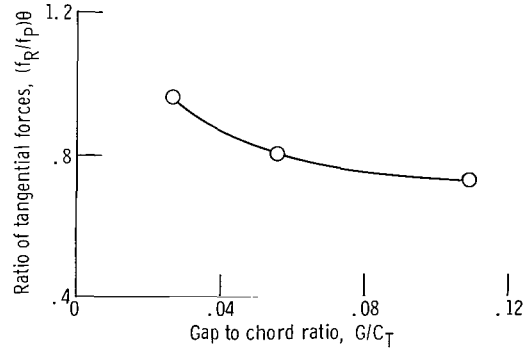

Figure 17. - Effect of gap on work split. Chord ratio, 1.0; camber ratio, 2.0; convergence, 1.4; overlap to chord ratio, 0.112.

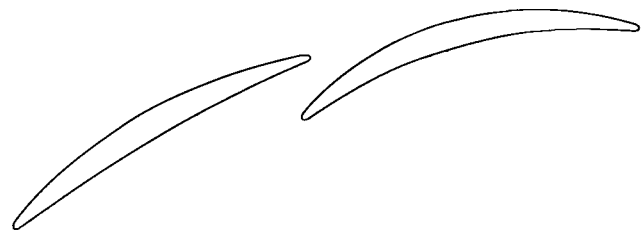

(a) Overlap to chord ratio, 0.053.

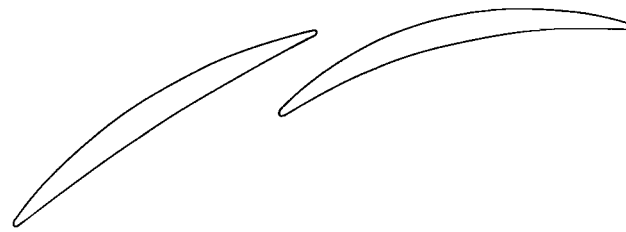

(b) Overlap to chord ratio, 0.112.

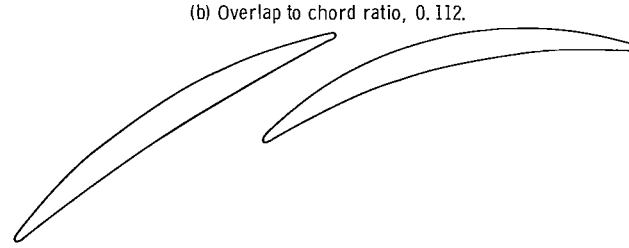

(c) Overlap to chord ratio, 0.178.

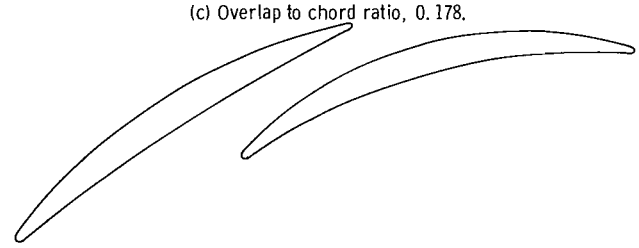

(d) Overlap to chord ratio, 0.251.

Figure 18. - Tandem blade section geometry: effect of overlap. Chord ratio, 1.0; camber ratio, 2.0; convergence, 1.4; gap to chord ratio, 0.056.

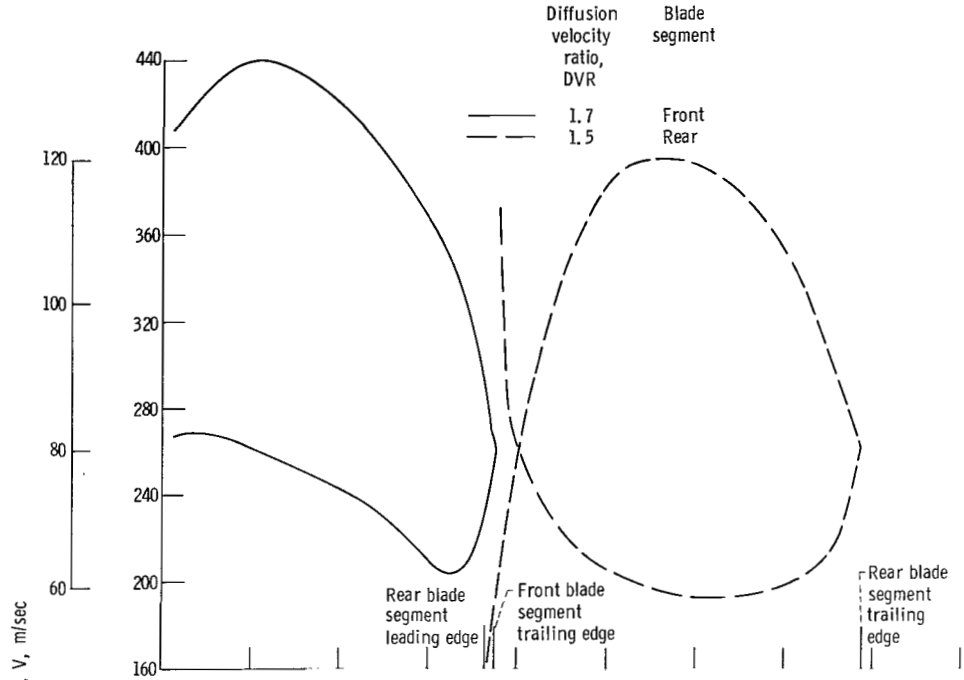

(a) Overlap to chord ratio, 0.053; $\kappa_{b-b} = -24.4°$.

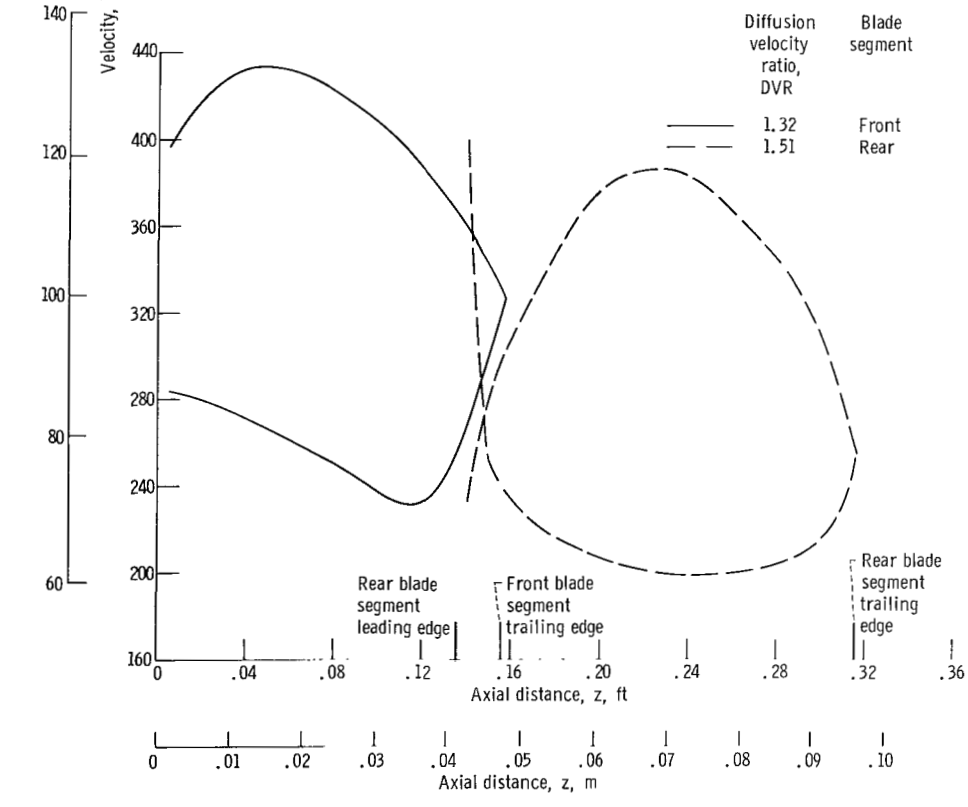

(b) Overlap to chord ratio, 0.112; $\kappa_{b-b} = -11.5°$.

Figure 19. - Effect of overlap surface velocity profiles. Chord ratio, 1.0; camber ratio, 2.0; convergence, 1.4; gap to chord ratio, 0.056.

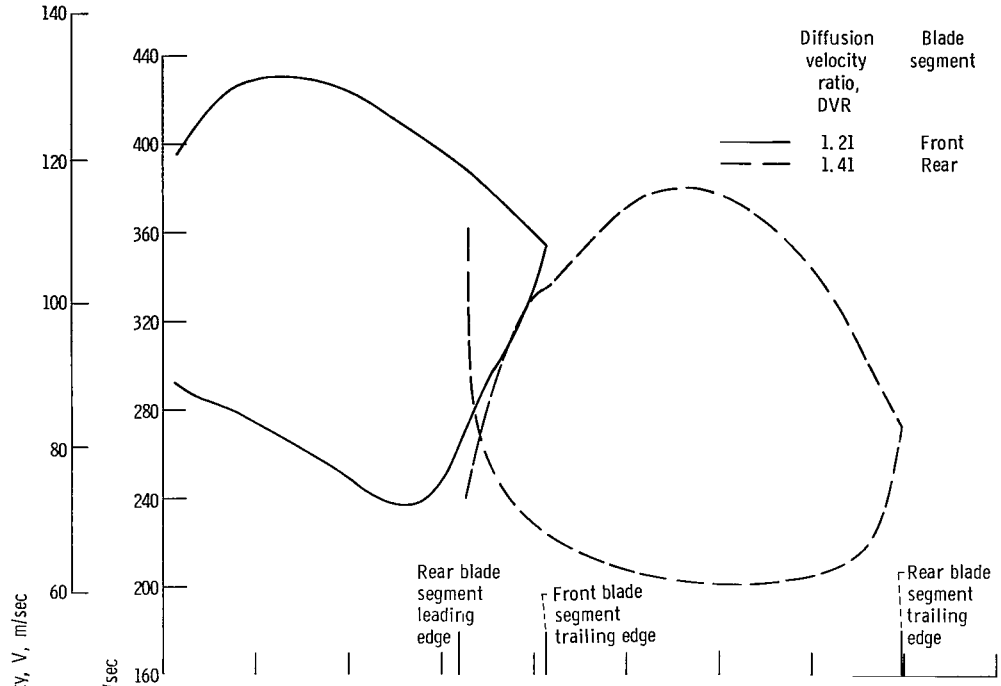

(c) Overlap to chord ratio, 0.178; $\kappa_{b-b} = -11.7°$.

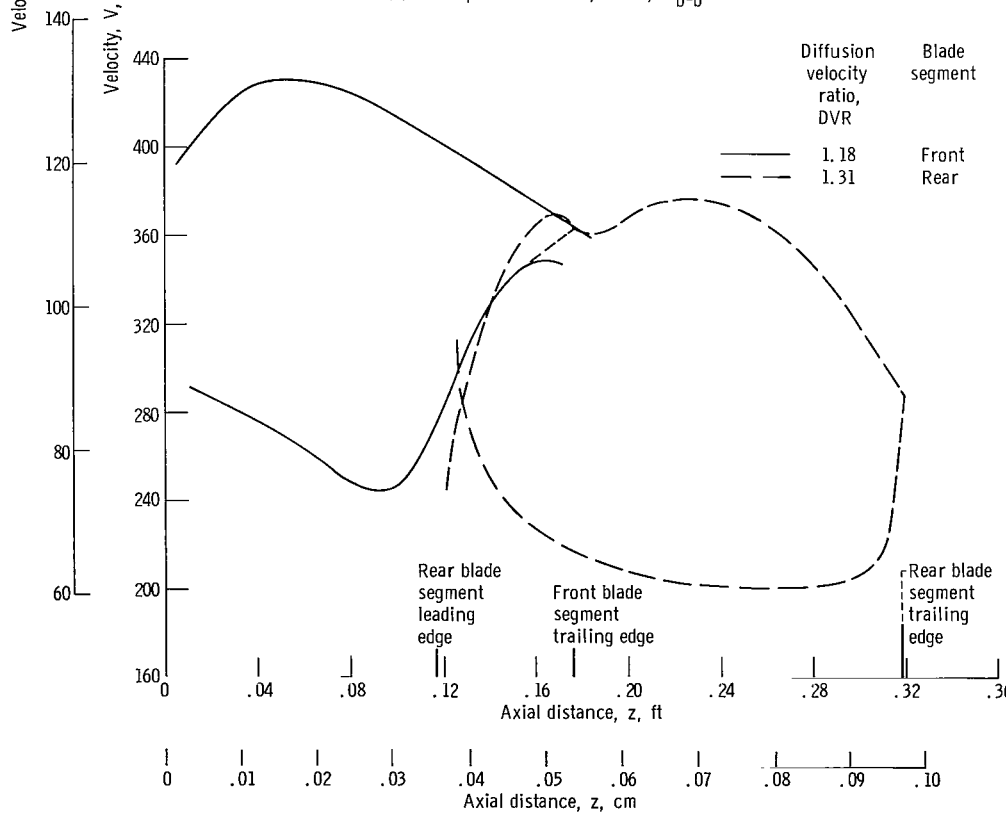

(d) Overlap to chord ratio, 0.251; $\kappa_{b-b} = -11.9°$.

Figure 19. - Concluded.

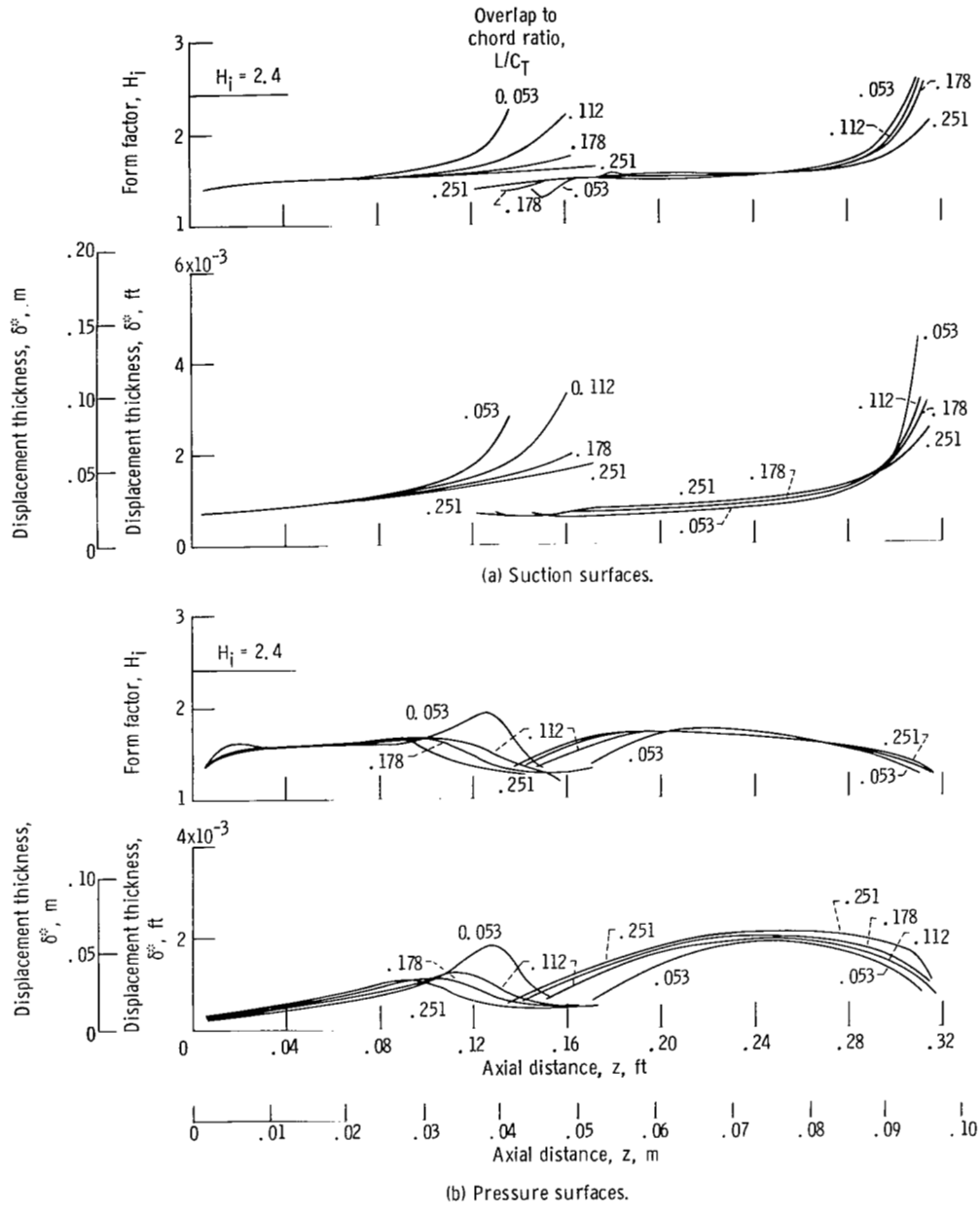

(a) Suction surfaces.

(b) Pressure surfaces.

Figure 20. - Effect of overlap on boundary-layer development. Chord ratio, 1.0; camber ratio, 2.0; convergence, 1.4; gap to chord ratio, 0.056.

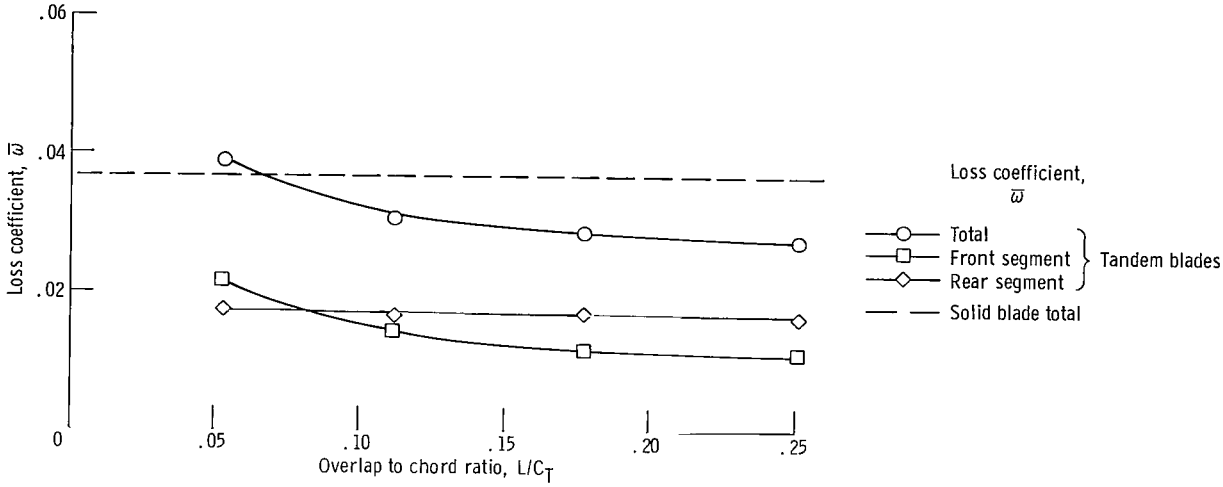

Figure 21. - Effect of overlap on loss. Chord ratio, 1.0; camber ratio, 2.0; convergence, 1.4; gap to chord ratio, 0.056.

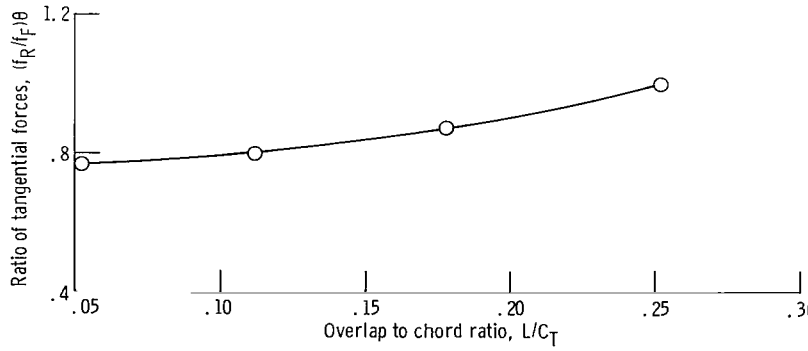

Figure 22. - Effect of overlap on work split. Chord ratio, 1.0; camber ratio, 2.0; convergence, 1.4; gap to chord ratio, 0.056.

(a) Camber ratio, 1.

(b) Camber ratio, 1.5.

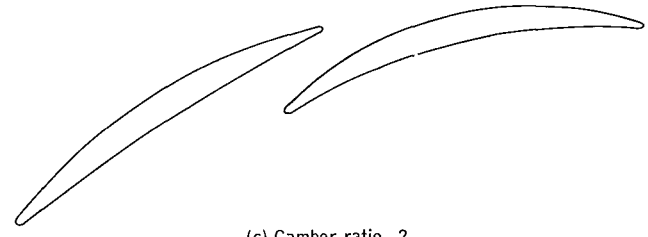

(c) Camber ratio, 2.

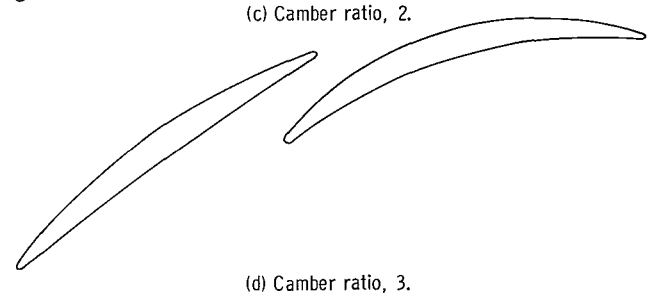

(d) Camber ratio, 3.

Figure 23. - Tandem blade section geometry. Effect of camber ratio. Chord ratio, 1.0; convergence, 1.4; gap to chord ratio, 0.056; overlap to chord ratio, 0.112.

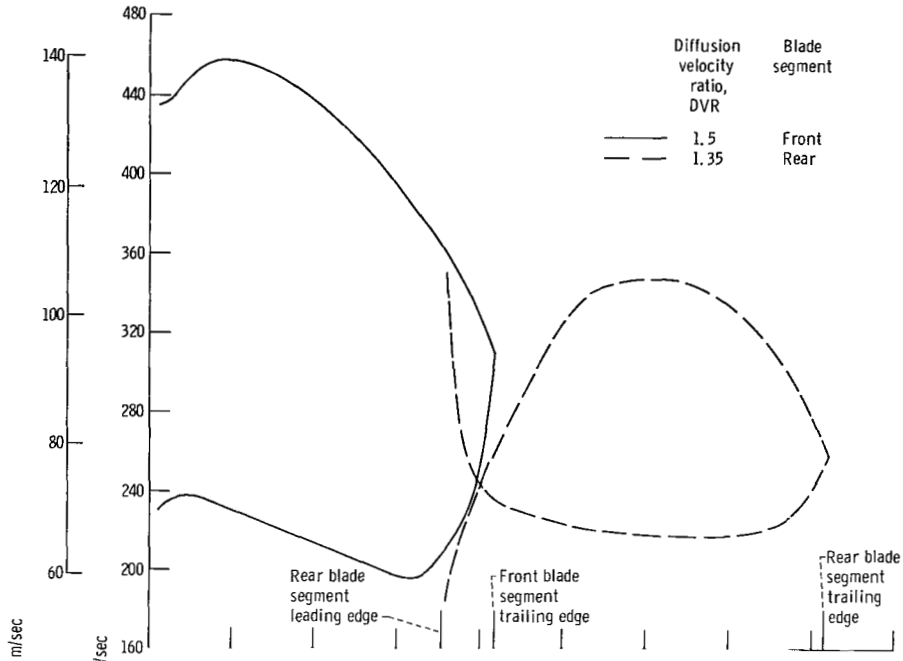

(a) Camber ratio, 1.0; $\kappa_{b\text{-}b} = -7.6°$.

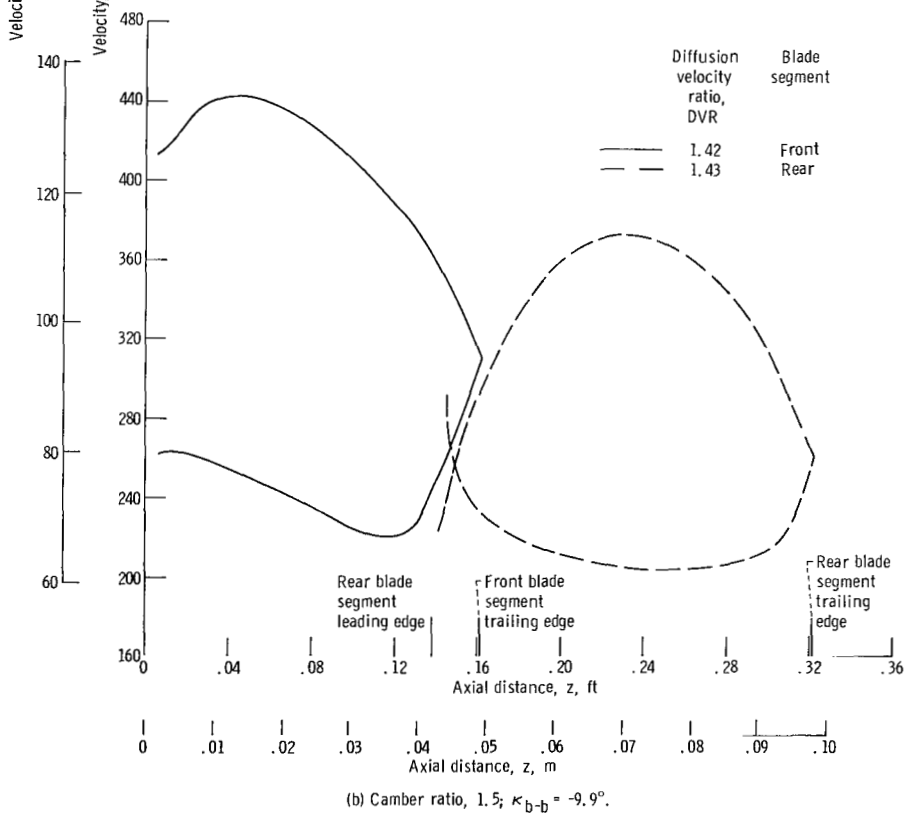

(b) Camber ratio, 1.5; $\kappa_{b\text{-}b} = -9.9°$.

Figure 24. - Effect of camber ratio on surface velocity distributions. Chord ratio, 1.0; convergence, 1.4; gap to chord ratio, 0.056; overlap to chord ratio, 0.112.

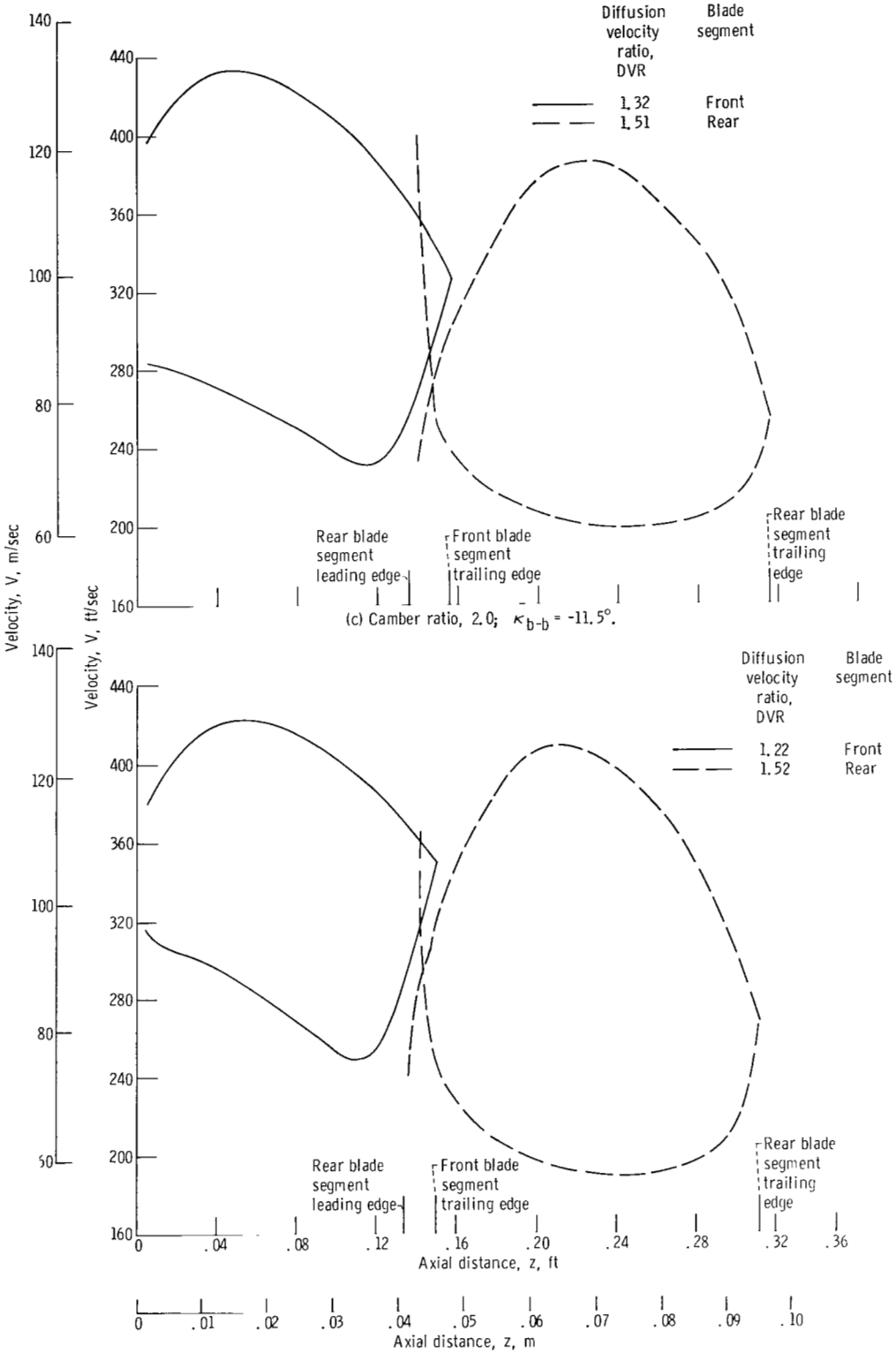

(c) Camber ratio, 2.0; $\kappa_{b-b} = -11.5°$.

(d) Camber ratio, 3.0; $\kappa_{b-b} = -13.3°$.

Figure 24. - Concluded.

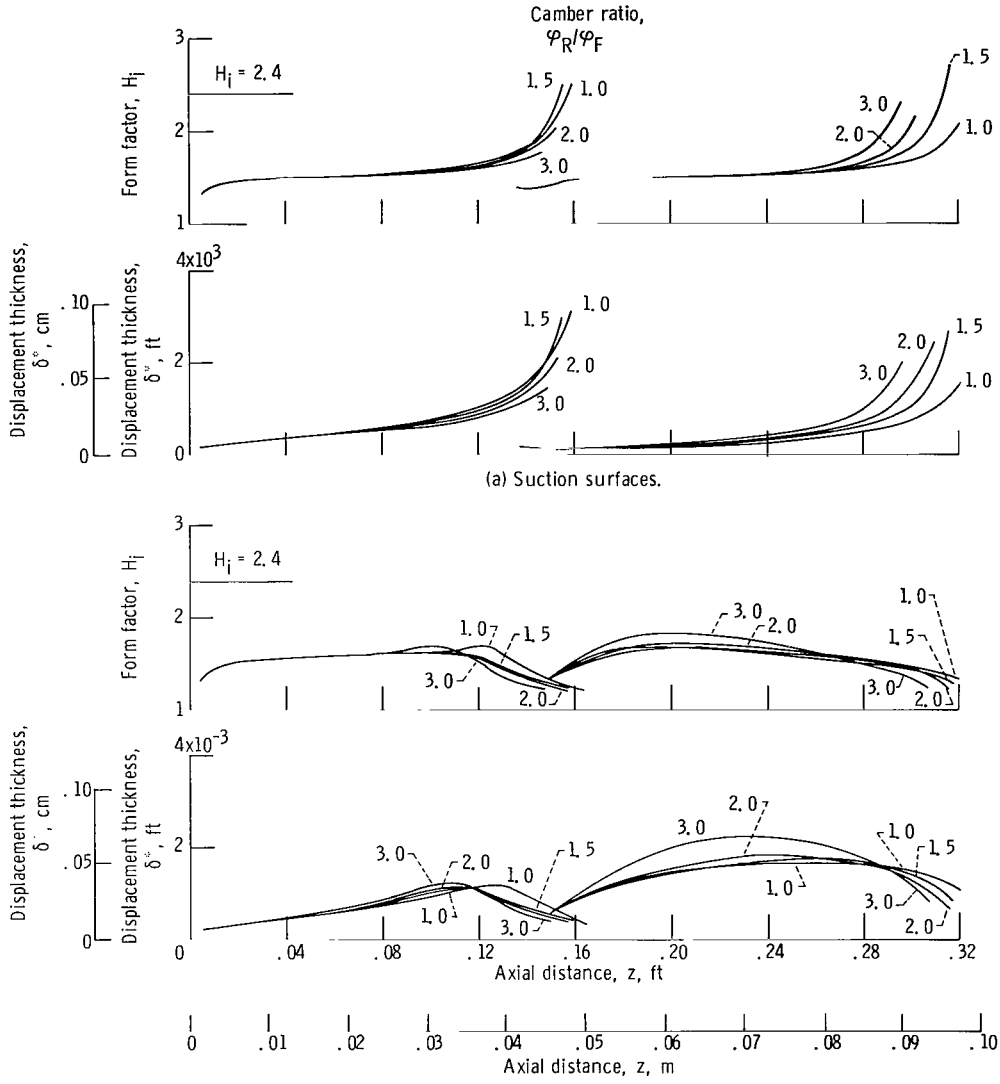

(b) Pressure surfaces.

Figure 25. - Effect of camber ratio on boundary-layer development. Chord ratio, 1.0; convergence, 1.4; gap to chord ratio, 0.056; overlap to chord ratio, 0.112.

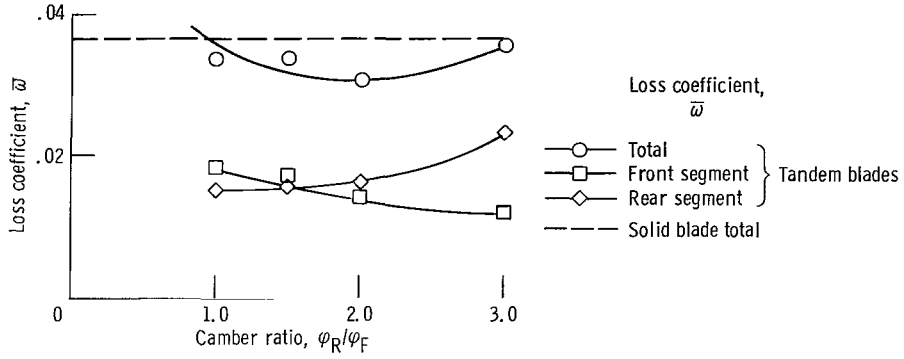

Figure 26. - Effect of camber ratio on loss. Chord ratio, 1.0; convergence, 1.4; gap to chord ratio, 0.056; overlap to chord ratio, 0.112.

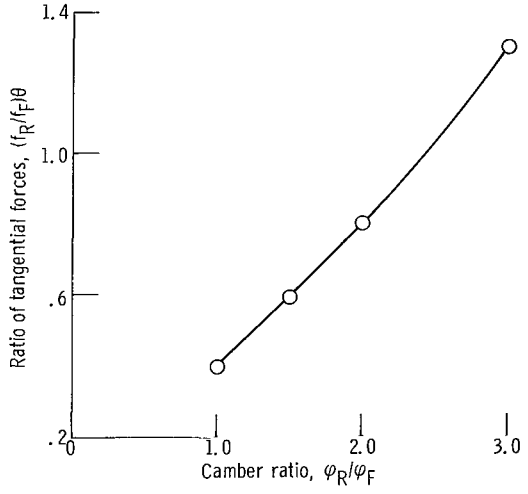

Figure 27. - Effect of camber ratio on work split. Chord ratio, 1.0; convergence, 1.4; gap to chord ratio, 0.056; overlap to chord ratio, 0.112.

(a) Chord ratio, 1.

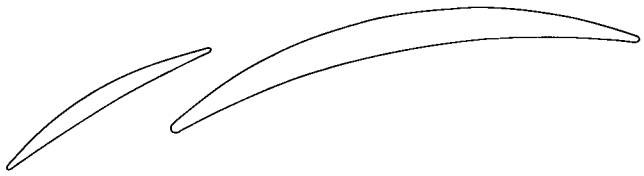

(b) Chord ratio, 2.

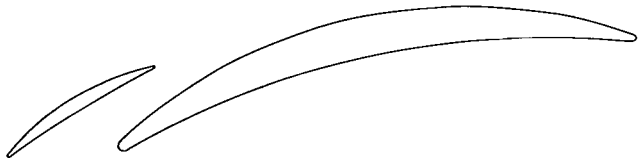

(c) Chord ratio, 3.

Figure 28. - Tandem blade section geometry. Effect of chord ratio. Camber ratio, 2.0; convergence, 1.4; gap to chord ratio, 0.056; overlap to chord ratio, 0.112.

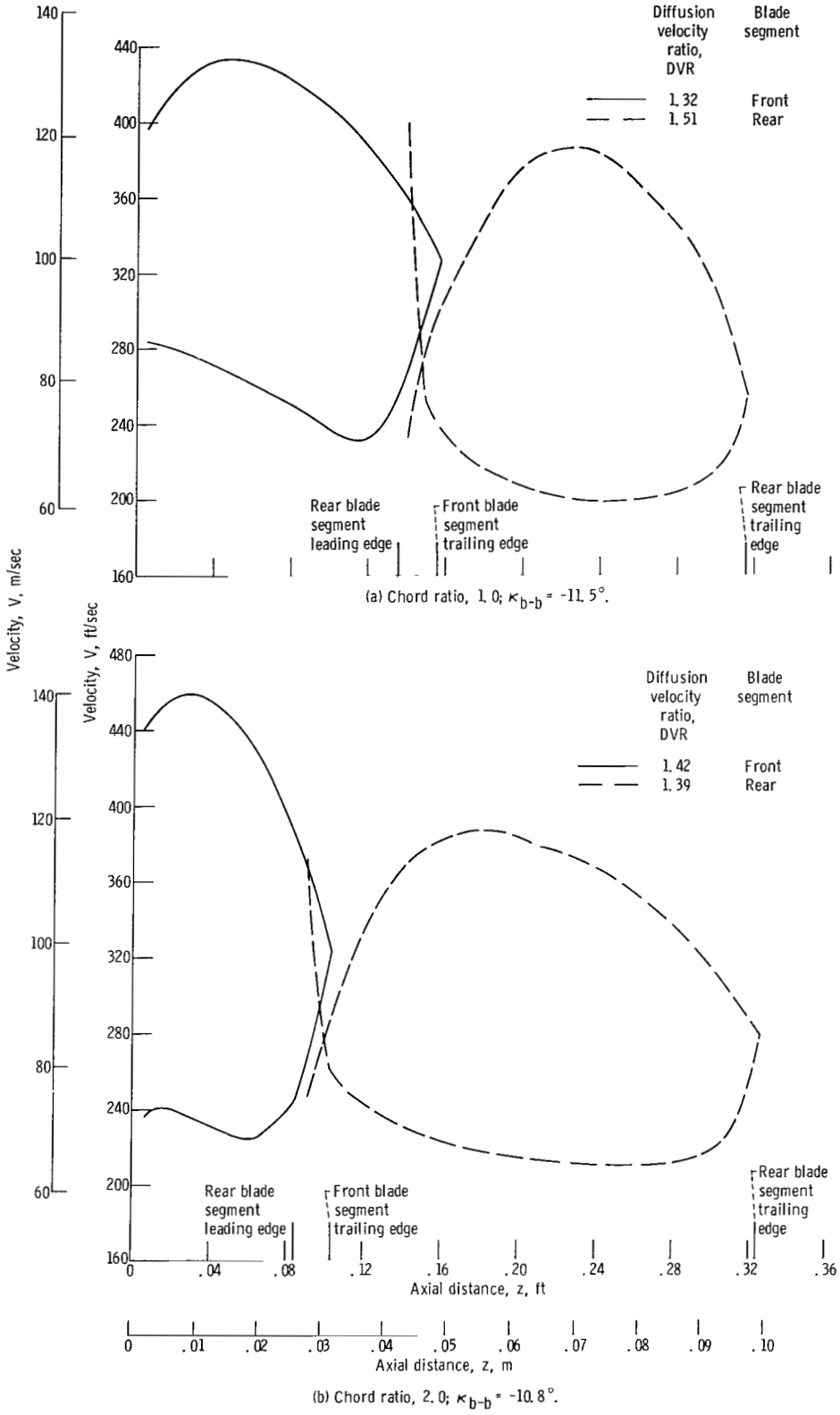

Figure 29. - Effect of chord length on surface velocity profiles. Camber ratio, 2.0; convergence, 1.4; gap to chord ratio, 0.056; overlap to chord ratio, 0.111.

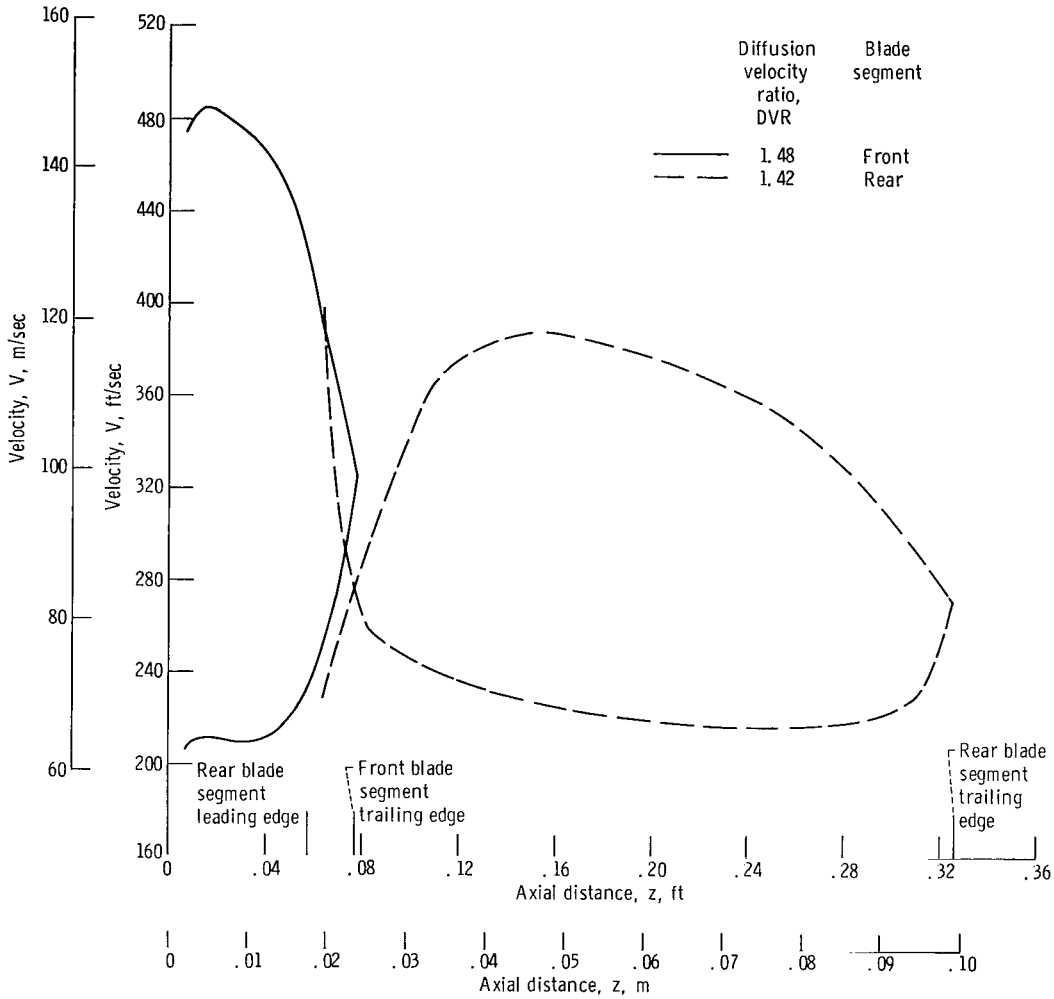

(c) Chord ratio, 3.0; $\kappa_{b-b} = -8.2°$.

Figure 29. - Concluded.

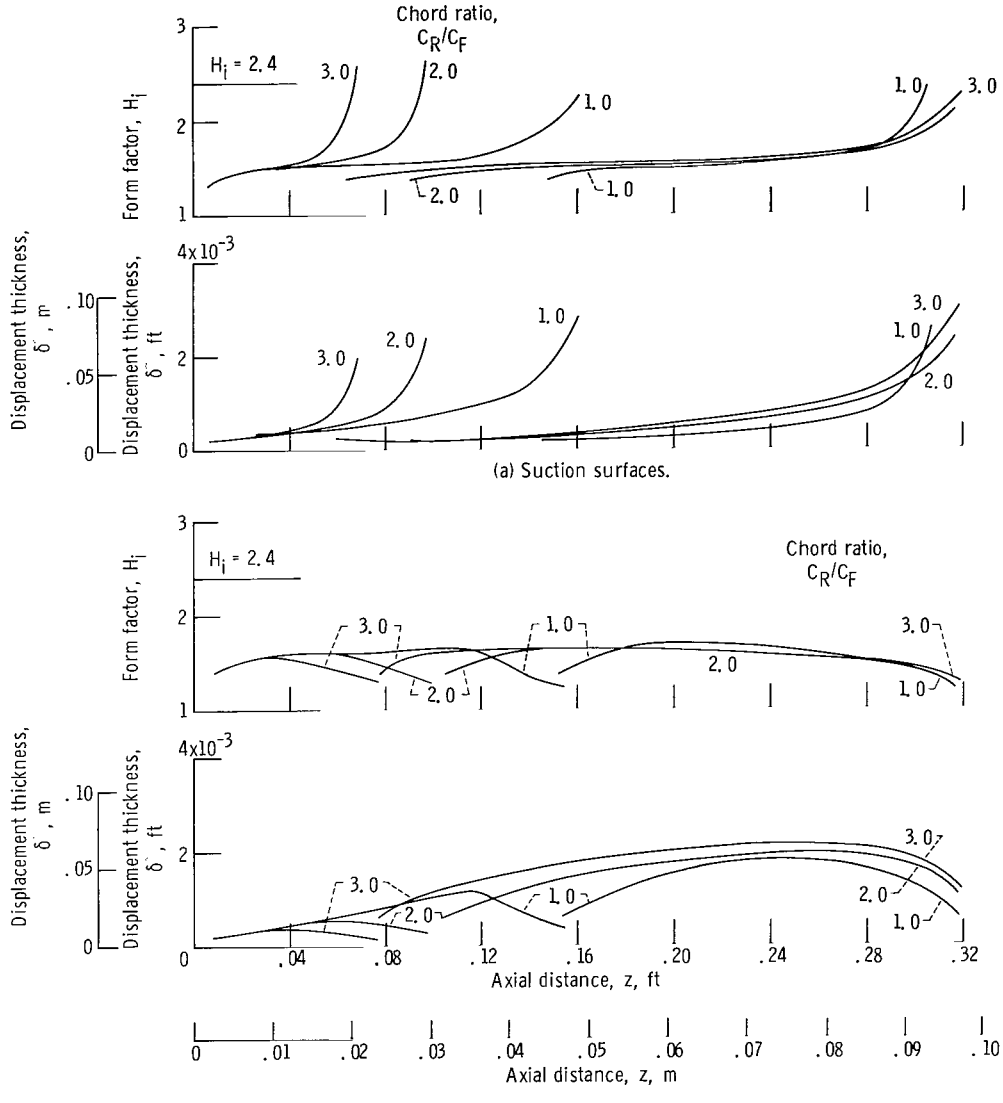

Figure 30. - Effect of chord ratio on boundary-layer development. Camber ratio, 2.0; convergence, 1.4; gap to chord ratio, 0.056; overlap to chord ratio, 0.112.

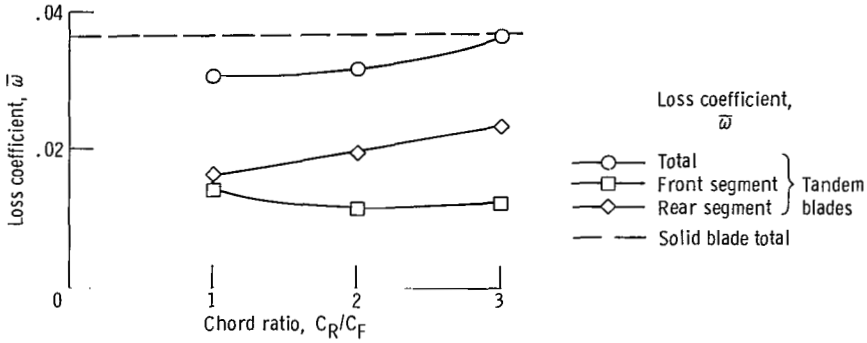

Figure 31. - Effect of chord ratio on loss. Camber ratio, 2.0; convergence, 1.4; gap to chord ratio, 0.056; overlap to chord ratio, 0.112.

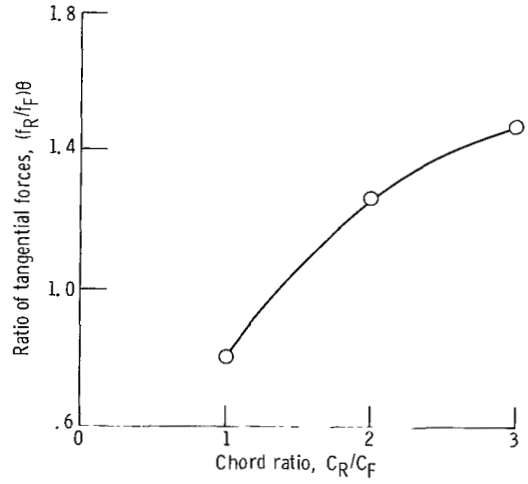

Figure 32. - Effect of chord ratio on work split. Camber ratio, 2.0; convergence, 1.4; gap to chord ratio, 0.056; overlap to chord ratio, 0.112.

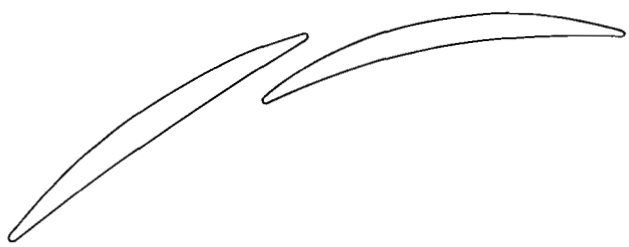

Figure 33. - Blade section geometry for low loss tandem blade. Chord ratio, 1.0; camber ratio, 2.0; convergence, 1.1; gap to chord ratio, 0.04; overlap to chord ratio, 0.11; $\kappa_{b-b} = -4.6°$.

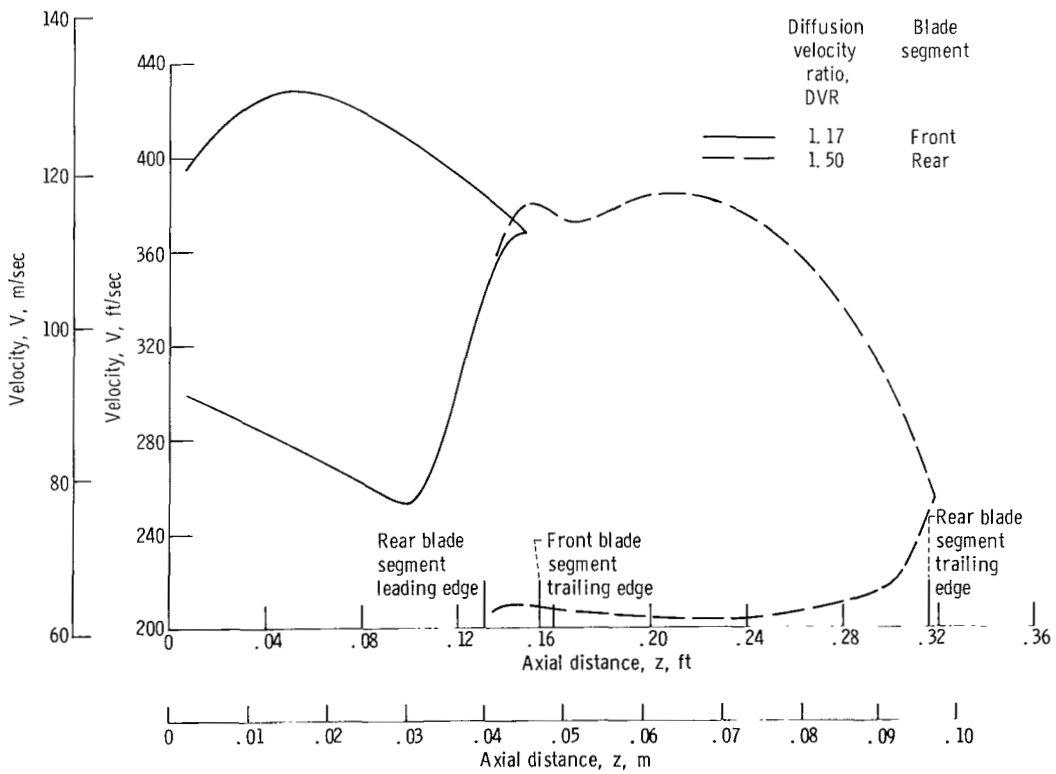

Figure 34. - Surface velocity profile for flow loss tandem blade. Chord ratio, 1.0; camber ratio, 2.0; convergence, 1.1; gap to chord ratio, 0.04; overlap to chord ratio, 0.11; $\kappa_{b-b} = -4.6°$.

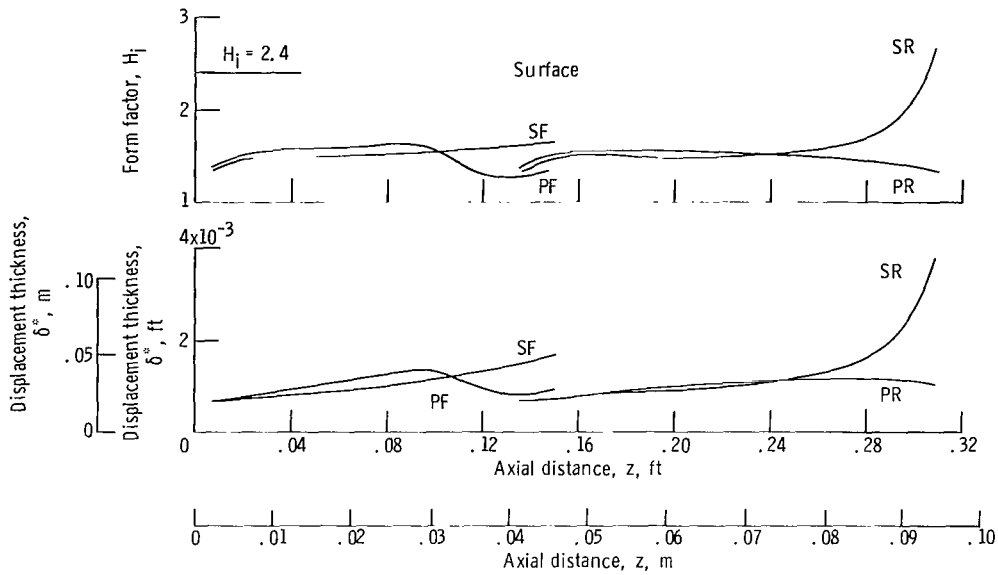

Figure 35. - Boundary-layer development on low loss tandem blade. Chord ratio, 1.0; camber ratio, 2.0; convergence, 1.1; gap to chord ratio, 0.04; overlap to chord ratio, 0.11.

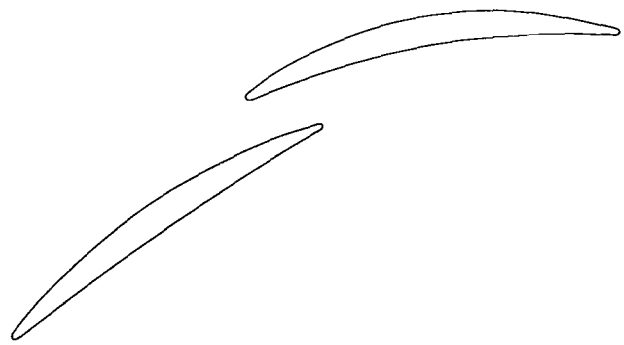

Figure 36. - Transposed tandem blade section geometry. Chord ratio, 1.0; camber ratio, 2.0.

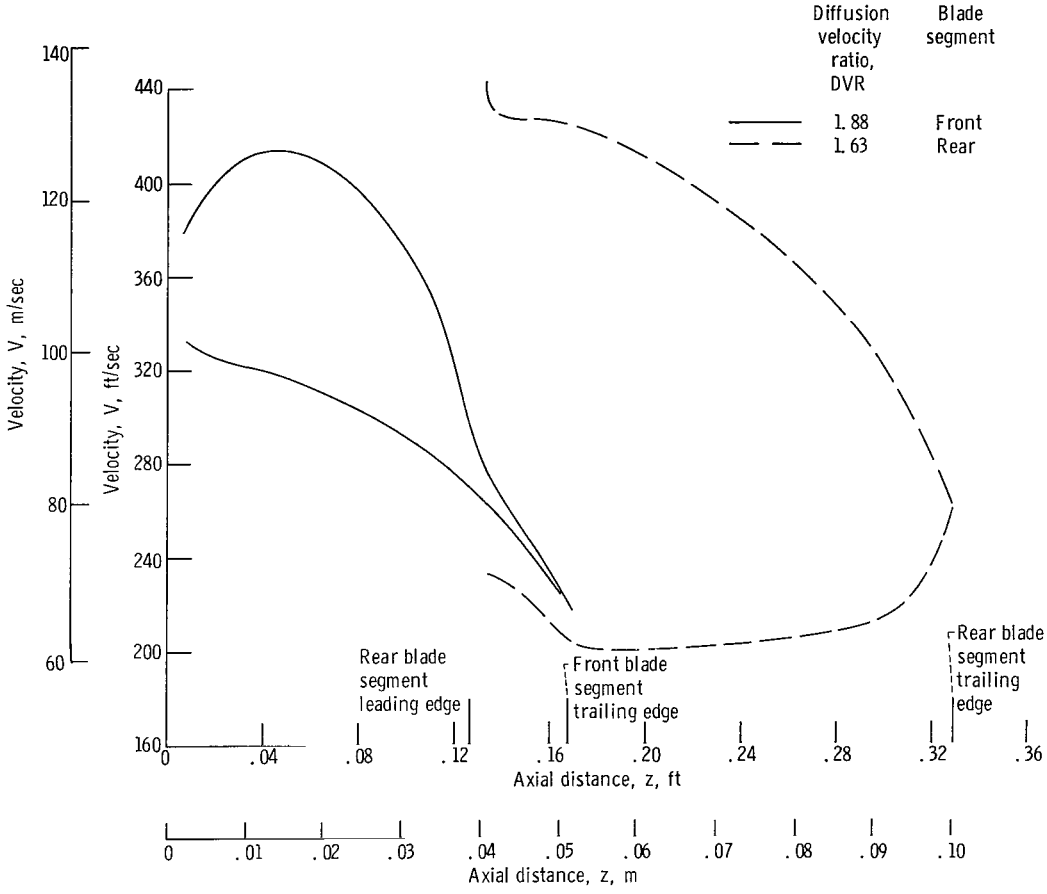

Figure 37. - Surface velocity profile of transposed tandem blade. Chord ratio, 1.0; camber ratio, 2.0.

NASA-Langley, 1971 — 1 E-5876